

## ANSWER TO REVIEWER 1

### General comments:

The study simulates an Antarctic cloud over the coastal Antarctic and the Weddell Sea in November-December 2015. Secondary ice production from the break-up of collisions between ice particles is added to Weather and Research Forecasting model. The model simulated results are compared to extensive measurements from airborne and ground-based instruments. Their results indicated break-up of collisions between ice particles could account for enhanced ice number in the pristine Antarctic atmosphere, and these results are insensitive to uncertainties in primary ice production. I think the study will be publishable after the following comments are addressed.

We are grateful to the reviewer for his/her comments that have helped us improve our manuscript.

### Specific comments:

1. My main concern is the experimental design. The control simulation is stated as using the default Morrison scheme (Line 204: “Additionally to the control (CNTRL) simulation, which corresponds to the default set-up of M05”). The Morrison scheme is described in the literature that includes different types of secondary ice production in it, i.e. the rime splintering (H-M) during snow accretion cloud droplets and snow accretion raindrops. Therefore, either I have misinterpreted and some additional description of the control model configuration is needed, or I think we need an additional set of control runs that have no secondary ice production processes included. Until there is a clean experiment with no secondary ice production processes it is difficult to interpret the statements about the impact of secondary ice production.

Thank you for this suggestion. The simulation with no SIP at all was initially included in the Supplementary Information, in the section that the sensitivity to the H-M process was tested. This test was referred as ‘CNTRL\_NOHM’, which corresponded to a simulation with the default M05 but with H-M deactivated. In the revised text we now refer to this simulation as ‘NOSIP’. Moreover, we have included the ‘NOSIP’ results in Figure 2, to help the readers quantify the impact of secondary ice production by comparing the rest of the simulations to ‘NOSIP’.

2. My first concern is about “separation size between ice and snow” The authors mentioned in the manuscript Line 215: “Note that since the separation size between ice and snow in the M05 scheme is 125  $\mu\text{m}$ , collisions that include cloud ice do not result in any multiplication in FRAG1siz.” The reader may be confused, does Morrison scheme really has a size separation between cloud ice and snow? Does this mean the model does not have cloud ice larger than 125  $\mu\text{m}$ , and no snow particles with a diameter smaller than 125  $\mu\text{m}$ ? Morrison scheme is documented in the literature that includes a threshold size (125  $\mu\text{m}$ ) for the cloud ice autoconversion process. But this does not mean a size separation between cloud ice and snow. Based on this, when comparing simulated snow and graupel with observation, does modeled snow and graupel only considering particles

larger than 80  $\mu\text{m}$ ? Or only modeled cloud ice has this threshold in size.

Thank you for pointing out this mistake. Cloud ice is converted to snow when diameter exceeds  $d_{cs}=125 \mu\text{m}$ . However since cloud ice (and snow) size spectra are represented with a complete gamma distribution, this means that sizes larger than 125  $\mu\text{m}$  are not excluded in the spectra (and, in fact, by the definition of a complete gamma function the sizes mathematically extend to infinity). However, if the characteristic diameter of the cloud ice category is larger than 250  $\mu\text{m}$  then all cloud ice is converted to snow in M05. Since break-up in FRAG1siz is allowed only if the characteristic diameter of the particle that undergoes break up is larger than 300  $\mu\text{m}$ , collisions with cloud ice do not contribute to multiplication. This statement is now corrected in the revised text (lines 219-221).

Regarding the modeled output plotted in Figures 2-3: when outputs are compared to observations, then only particles larger than 80  $\mu\text{m}$  are accounted for consistency with the cloud phase detection limit in the observations; this holds for model data plotted in Fig. 2 and Fig. 3a,c,d. In Figure 3b, graupel is not compared to observations, so we plot the whole graupel spectrum to show how limited its concentration is. This is better explained in the revised text (lines 282-290) and Figure caption to avoid confusion.

3. Related to the second concern, the third concern is related to the comparison between observation and model results. The authors mentioned that “consistency with M05, the threshold size separating measured cloud ice from snow is set to 125  $\mu\text{m}$ ” Usually, when comparing model ice with observation, we added different types of modeled solid particles together, then using the total mass and total number to compare with the observed IWC and ice number concentration. Because it is hard to tell cloud ice from snow in observation data. I suggested using a similar method when compare the modeled ice number with observation.

We have corrected the adapted threshold in this figure; this is now set to 250  $\mu\text{m}$  for consistency with the microphysics scheme assumptions (see answer above). Although it is hard to separate cloud ice/snow in observations, 2DS measurements offer a good indication of the size spectra. Plotting cloud ice and snow categories separately in this figure is important, because it shows that including break-up in the scheme results in more realistic representation of the microphysical properties. Particularly, it is important to show that it is the concentration of the small particles that is substantially underestimated in the control simulation (more than 2.5 orders of magnitude, see Figure 3a); concentration of large particles ( $>250 \mu\text{m}$ ) is underpredicted by less than a factor of 1.5 (see Figure 3c). Thus, break-up shifts the modeled size spectra towards smaller values in agreement with observations, which indicates that we are likely capturing the correct mechanisms responsible for the ice microphysical characteristics. This is now discussed in lines 302-307. We have also included a fourth panel in this figure, to show the vertical profiles of total ICNCs.

4. The fourth concern is related to parameterization from Phillips et al. (2017) In the sensitivity test, Line 255, “These simulations are referred to as PHIL0.2, PHIL0.3 and PHIL0.4 in the text, where the number indicates the assumed values of  $\Psi$ ”. In the bulk microphysical scheme, snow is referred to as dry snow, with smaller density (prescribed and fixed in the scheme), graupel is rimed ice with larger

density. Setting the same rimed fraction for different collisions is not consistent with the assumptions in the microphysics scheme. I suggested the uses different rimed fraction for snow-snow and graupel-graupel collision. The rimed fraction could be changed in the sensitivity test, but in one simulation, the rimed fraction for the collision between snow-snow should not larger than rimed fraction for the collision between graupel-graupel.

We apologize for this confusion. In the Phillips parameterization, graupel particles are highly breakable as  $\Psi$  is assumed to be larger than 0.5; the fragment generation does not depend on  $\Psi$  and is only a function of temperature (see equations at line 622 in Appendix B). In contrast,  $\Psi$  is important for cloud ice/snow and that's why fragment generation directly depends on  $\Psi$  for these ice categories (equations in line 609). The parameterization assumes that  $\Psi$  for these ice types is less than 0.5, lower than for graupel, in agreement with the reviewer's comment.

The different assumptions regarding the rimed fraction of graupel and the rest of the ice categories are now discussed in detail to avoid confusion (lines 229-235 in the revised text). It is also explicitly stated that variations in  $\Psi$  only affect the break-up efficiency of cloud ice/ snow.

5. The last one is related to radiation. Does cloud microphysical properties couple with radiation transform code? It is interesting to see the model has a larger ice number and IWC, after the implementation of the secondary ice process, but the longwave radiation does not change accordingly. How about the effective radius of the ice particle? Does it change after the model has secondary ice production in it?

This is an excellent point. Only the mass mixing ratios of liquid and ice particles are transferred to the radiation scheme and drive the differences reported in Table 1. No information on effective radius is directly passed to RRTMG scheme. This is now clarified in the text (lines 323-325).

### **Technical corrections**

1. Line 59 "Lachlan-Cope et al., 2016; Wexx et al.,". Wexx →Wex?  
Although the statement was more general about polar clouds, we have removed the reference 'Wex et al' since this concerns Arctic clouds
2. Line 96 be → been  
corrected
3. Code and data availability: the link authors provide does not link to the measurement data, please upload the data.  
We apologize that the direct link did not work in the previous manuscript. However, the provided URL address is valid. Hopefully, the link works fine in the revised version (in any case copy-pasting the address in a browser should definitely work)

### **Comments embedded in the pdf version of the manuscript**

The reviewer points out that strong riming is the foundation of the hallet-mossop process. This sounds somewhat contradicting to our findings regarding the fact that only simulations that assume a high rimed fraction for the particles that undergo

break-up during ice particle collisions produce realistic ICNCs, while at the same time H-M remains inactive.

While in Phillips parameterization for break-up, rimed fraction is explicitly considered, this is not the case for H-M. To make sure that only sufficiently rimed particles contribute to multiplication, H-M is activated only if the ice particle mixing ratio exceeds  $0.1 \text{ g kg}^{-1}$ . However, this threshold is ad-hoc and is tuned for mid-latitude clouds, but is hardly exceeded in polar clouds. In the former submission we discarded the liquid thresholds in the parameterization and found no impact on the results. In the revised manuscript, we removed both liquid and ice thresholds and allowed H-M to be active over the whole droplet and snow/graupel spectrum. This enhances the H-M efficiency by a factor of 3 but still cannot reproduce observed mean ICNCs. This set-up overestimates H-M efficiency, as size limitations have been reported in laboratory studies, but the existing thresholds in M05 should be refined for polar clouds. The whole text has been moved from the Supplementary Material to the main manuscript (section 4.3).

### **ANSWER TO REVIEWER 3**

#### **General Comments**

This is a good paper overall, in its seeking to explore the role of different secondary ice formation mechanisms active under conditions present in clouds over the focused region near Antarctica. To the extent that I can tell, the findings with regard to BR parameterizations are solid and enlightening regarding the necessary conditions (especially heavy riming) for it to occur and the need for formulations of BR that account for the requisite size of colliding particles

We are grateful for the many insightful comments that have helped us improve our manuscript.

This paper was less forward and unsatisfying in conveying that end-to-end prediction of secondary ice formation actually still eludes the community. This is my inference from this paper and from the literature of the last few years represented by some of the team on this paper. This relates to the assumptions on primary nucleation, and the concentrations of ice that exists outside of regions where strong SIP ensues. There is still a gap here, one that is not really discussed, although this study seems to close it some. By this I mean that the authors have proposed to explain how ice concentrations go from values of 0.1 per liter to ones enhanced up to 100 times, and under conditions that the Hallett-Mossop process cannot explain such enhancement. The results cannot explain the inconsistency between recent INP measurements over the Southern Ocean or near Antarctica (e.g., McCluskey et al., 2018; Schmale et al., 2019; Welti et al., 2020) and the fact that Litkowski et al. (2017) required use of the DeMott et al. (2010) parameterization (with qualifications about its likely inapplicability to the region) in order to explain consistency with at least some of the ice concentration signature in the regional clouds.

The summer coastal low-level Antarctic clouds are dominated by supercooled liquid droplets while ice occurs in isolated large ice patches. Our statistics that focus on cloud ice properties by default refer to the ice-containing regions of the cloud. This

indeed was not clear in the initial version of the manuscript and now is explicitly mentioned in the abstract, case description and conclusion section.

Although no primary ice scheme is likely suitable for polar conditions, DeMott et al. (2010) still performs better than all other parameterizations available in WRF (and generally in models with no prognostic aerosols). This was discussed in Listowski et al. (2017). Sensitivity tests however are considered to address the factor of 10 uncertainty in the chosen parameterization, but we acknowledge that the results of these tests were not emphasized enough in the main manuscript and particularly the large sensitivity to INP reductions. For this reason the whole section on primary ice nucleation has been moved from the Supplementary Material to the main text (section 4.4). The fact that a minimum primary ICNC concentration of  $0.1 \text{ L}^{-1}$  is needed to initiate break-up is now explicitly stated in both ‘abstract’ and ‘conclusions’ section. Potential suggestions on how this requirement might be met are offered in sections 4.4 and 5 (e.g. ice seeding as likely in our case, transport of terrestrial aerosols, more efficient H-M).

Moreover, the deficiencies of the applied parameterizations, such as the fact that they have been neither developed or calibrated for polar conditions, are also explicitly mentioned in the revised text (lines 399-404, 499-500).

The measurement issue is that it seems that many of the clouds remain supercooled or perhaps with ice in them at a level that could elude measurement due to detection limits. The initial transition to the point that calculations start in this study is unexplained. This does not greatly harm the paper, since it remains as a mystery for many investigators. However, some simulations performed (CNTRL case primary ice decreased by 10x) make it clear that BR would not occur in clouds with lower primary ice concentrations. This deserves some mention/discussion in the main manuscript. There must be “enough” ice, enough apparently being 0.1 per liter in the temperature regime between 0 and  $-9^{\circ}\text{C}$ , and then BR can ensue and, if done properly, explain ice enhancements observed in many cases. But primary ice nucleation appears not capable of providing that starting ice concentrations, based on available information. I reiterate this point in some of the specific comments below.

The sensitivity in low INP conditions is now discussed more extensively in section 4.4 and the fact that there might be a ‘triggering’ primary ICNC threshold that can explain the observed ice patches within the predominately liquid clouds. Furthermore we discuss possible processes that can provide the necessary conditions to meet this requirement (e.g. ice seeding in the particular case). This finding is also repeated in the ‘conclusions’ section.

### Specific Comments

#### **Abstract:**

**Lines 27-28:** In what studies has primary ice formation ever been constrained in the region of this study by aerosol measurements? To me it implies that someone has reliably connected aerosol measurements and ice nucleating particle measurements to primary ice formation measured in the region.

The abstract has been modified substantially and this sentence has been removed.

**Lines 30-32:** To be explicit, the parameterization bridges the gap between measured ice concentrations outside of SIP regions (perhaps, this is not clearly shown) and ice concentrations ultimately achieved in some areas.

By default ice properties are only calculated with the observed ice patches where SIP seems to occur. To avoid any confusion this is now explicitly stated in the abstract along with the fact that these ice patches are observed within predominantly liquid cloud layers.

**Line 33:** “Insensitive to uncertainties in one primary ice production parameterization.” Or something to that effect. Without a clear understanding of primary ice formation in these clouds, one cannot claim that the uncertainties or concentrations are known. Given that some observations have not been mentioned, I suggest that qualification be made that end-to-end understanding still eludes the field. What the paper shows, and what is not made clear here, is that this is true as long as some other primary or secondary process is able to produce 0.1 per liter ice to begin with. Unfortunately, none is known to exist. It is wired into the model via use of a parameterization that has not been constrained by INP observations in this region.

We now make clear in both abstract and ‘conclusions’ section that a minimum primary ice concentration of  $0.1 \text{ L}^{-1}$  is needed to initiate break-up. Potential contributions to this minimum value are also mentioned in section 4.4. and 5.

**2) Introduction: Line 53:** Suggest “: : generation of ice crystals in a cloud that: : :” ...ensues following primary ice nucleation, but occurs in large excess to ice nucleating particle (INP) concentrations: : Otherwise this seems an awkward definition. It does require INPs or pre-existing ice from some nucleation process, but the key factor is that it far exceeds these initial values in concentration.

The whole paragraph has been revised (lines 51-55).

**Line 77-78:** Suggest that “it is” and “it” can be removed from this sentence for readability. Also, please note that neither of the referenced studies in this sentence were for the region of study, and the latter should be qualified as a modeling study.

Thank you, corrected

**Line 103-104:** This statement does not describe the results herein or in Young et al.(2019) in my opinion. They state, my emphasis added, "Under the assumption that primary ice is suitably represented by the model, we must enhance SIP by up to an order of magnitude to simulate observed Nice!" They did not observe INPs, correct? To be accurate, “: : help to explain: : :”? Also it is important to note that this study will also not use observation of INPs as a basis for any sort of closure on complete understanding. The implementation in the Morrison scheme does require explaining the suitability of the inherent ice nucleation scheme, and so it was appreciated to have an Appendix relating to that.

We have modified this statement, which was inaccurate, by referring now to the discrepancy between observed and modeled ICNCs in line 101 (instead of INPs and ICNCs).

**Line 149-154:** ICNCs were substantially higher than what? The model ice? Expectations? Based on what? Just for reference, the ICNCs quoted here for the noted temperature range are not one order of magnitude higher than expectations based on more recently reported INP measurements in the Southern Hemisphere ocean region



(references noted above), and are 3 orders of magnitude higher than Bigg (1973) at the nearest temperature of observation. Also, regarding noting the “frequency” of observations of low aerosol concentrations and high ICNCs, are you failing to acknowledge the other publications on the observational studies that indicate the apparently more frequent observations of supercooled water conditions? What I am getting at is being clear on what part of the discrepancies are endeavored to explain here, how one gets to these concentrations and from what level of ice presence. The model predicted values, or the diminishingly low values one might expect from observations of INPs? Is it possible to state what the lower detection limits for ice concentrations are in observations, and how this might affect the mean values or spread in ice concentrations?

Although clearly INPs can be substantially lower over the Southern Ocean, we do not have INP measurements for the particular case. For this reason we only state the aerosol concentrations available to indicate how clean is the measured atmosphere. Assuming that the average of observed INP from the literature is more representative for our case than INP diagnosed from direct aerosol observations (with uncertainty of one order of magnitude) is also subject to considerable uncertainty. Considering the high ICNC conditions in the observed cloud ice patches, surface INP measurements may not account for ice-nucleating particles transported above/within the cloud.

When calculating ICNC statistics, by default this estimate concerns the ice-containing regions of the cloud. However, we acknowledge that this was not explicitly discussed in the previous version of the paper.

Regarding detection limits, the 2DS is a single particle instrument: it measures all particles that pass through its sample volume with size larger than  $\sim 10 \mu\text{m}$ . However phase identification cannot be conducted for particles with sizes lower than  $80 \mu\text{m}$ . The 2DS sample volume depends on particle size and the data integration period. For example at  $300 \mu\text{m}$  the sample volume is  $3.7 \text{ L/s}$ . For 1 count measured within 1-sec averaging window, this equals a concentration of  $0.27 \text{ L}^{-1}$  (  $1 \text{ count} / (3.7 \text{ L/s} * 1 \text{ s})$  ). If a 10-sec window was chosen, then this value would go down to  $0.027 \text{ L}^{-1}$ . There is an uncertainty in the concentration due to the counting statistics ( $1/\text{sqrt}(\text{counts})$ ). For 1 count the uncertainty due to counting statistics is 100 %. This is now explained in section 2.1, lines 121-125. The total uncertainty in ICNCs is even larger but cannot be determined. However, what the applied thresholds ensure is that calculations concern ice patches, not liquid-only regions (line 243-244), and that this is consistent for both observations and model.

**3) Modeling Methods General comment on this section:** I found it very confusing to have two of the altered simulations refer to alteration of size dependencies, but in one for the limitation to be that crystals exceeded a certain size (FRAG1siz) and the other to required that size be scaled for a very large size to one much smaller (TAKAHsiz). I have no recommendation for describing size effects that are totally different.

We changed TAKAHsiz to TAKAHsc (to indicate scaling for size)

**Line 226, end of Section 3:** The abstract mentions sensitivity tests on primary ice nucleation. I understand that these are given in the Supplemental, but this should perhaps be mentioned here.

The whole primary ice section has been moved from the Supplementary Information

to the main manuscript as section 4.4.

#### 4) Results

**Line 240:** The CNTRL simulation underestimates mean ICNC, but it should be made clear that this is because of the misrepresentation of the highest ICNC, correct?

Yes, as now stated in lines 268-269 CNTRL cannot reproduce the whole spectrum and largely underestimates the frequency of ICNCs  $> 1 \text{ L}^{-1}$

**Line 342-344; lines 352-353:** This is not really the potential uncertainty in INPs, right? This is the uncertainty for the parameterization. That parameterization does not have representation in samples from either Antarctica nor from marine boundary layer regions. The reason this becomes important is the final statement “: : as long as there are enough crystals to initiate this process.”

The discussion in section 4.4 now addresses the fact that the parameterization is not constrained based on Antarctic measurements. The fact that a minimum primary concentration of  $0.1 \text{ L}^{-1}$  is required to initiate BR is now emphasized throughout the whole manuscript.

If INP number concentrations are exceedingly low, as they appear to be in some recent studies referenced above, is the BR process ever stimulated unless cloud tops get much colder? It seems not. It seems that some other process is needed to explain the presence of something on the order of 0.1 per liter already at all temperatures warmer than  $-9$  ? Based on Fig. S4, I ultimately noticed that the basis of your statement must be in the simulations where INPs were decreased by a 10x factor. In that case, it appears that the BR process does not come into play. This is an important finding in my opinion. It deserves mention as another key result.

This is now mentioned as a key result. We also suggest processes that might result in conditions favorable for BR (e.g. ice seeding, aerosol transport). It is likely that understanding the interactions between such processes might explain the reason why large ice patches with substantially enhanced ICNCs are observed when supercooled liquid cloud conditions generally dominate.

**5) Conclusions Lines 356-360:** The results indicate that if sufficient ice concentrations are present already, or are parameterized to be at a certain level, then BR can do what is stated here. However, primary ice nucleation is not “limited” in this study. It is far in excess of existing INP measurements

The conclusion section now emphasizes that certain primary ice conditions are required to initiate BR. We also explicitly state that such INP conditions are not frequently found over Southern Ocean, which is likely the reason why supercooled droplets dominate in these clouds.

#### Appendix A

**Lines 392-393:** The Meyers et al. (1992) formulation for contact freezing is another parameterization of questionable applicability to this region. Ignoring that or whether it contributes at all or not, I am unclear on what is meant by the rates being further weighted by the effective diffusivity of the contact nuclei. You mean an altered assumption is made on their size? Or how size impacts scavenging rate? Please explain.



The effective diffusivity of the contact nuclei is estimated based on Brownian motion as (similar to Young 1974):  $D_{ap} = R T (6 p r_i N_A m)^{-1} [1 + 0.0737 T (2880P)^{-1} r_i^{-1}]$ , where  $R$  is the universal gas constant,  $N_A$  is Avogadro's number,  $m$  is the dynamic viscosity of air,  $T$  is the temperature,  $P$  is the air pressure, and the radius of ice nuclei  $r_i$  is assumed to be  $1 \times 10^{-7}$  m. The factor in the brackets  $[\ ]$  is a correction factor accounting for the mean free path of air molecules relative to the size of the ice nuclei (all units are MKS). This information is now provided in the revised manuscript in lines 488-493

**Lines 397-398:** If the parameterization for heterogeneous nucleation has been selected to compare better with in-cloud ice measurements over the Antarctic Peninsula, does that not “fix” the primary nucleation problem, without necessarily knowing if this is disguising other processes that must be at play to achieve such concentrations? Given what I mention already above, you might need to explain that this selection has been made to solve an issue or is perhaps based on some prior inference that these ICNCs must be the INP concentrations, not because it is the most appropriate thing to do. This is discussed in some of the papers that preceded this one, especially the fact that the parameterization selected was not relevant for application on sea spray particles.

Previous comparisons of this scheme and other primary ice nucleation schemes available in WRF for Antarctic Clouds have shown that the Cooper parameterization performs worse (Listowski et al. 2017). This is also the case for Arctic clouds (Young et al. 2017). Nevertheless, DeMott's and Cooper's schemes produce similar primary ice over the temperature range covered by the observations, but the latter provides unrealistically high values at lower temperatures (see Young et al. 2017 and Supplementary Information of Young et al. 2019). This is now explained in Appendix A (lines 496-504).

### **Figures**

**Figure 2:** It is only here that some limitation on ice at 0.005 per liter is mentioned. Apparently, this is the minimum ice concentration accessible at some measurement frequency, due to sample volumes I assume. This is nowhere explained, but it should be reiterated here. This limit also sets the limit on what is referred to as supercooled water versus ice. What if this were set at 0.00005 per liter, which may be closer to what could be available as INPs? Yet in this figure, it somehow looks like there is a threshold around 0.2 per liter. Why is that?

1 count measured by 2DS within 1-sec averaging window corresponds to a concentration of  $0.27 \text{ L}^{-1}$ . This was the minimum concentration in our previous manuscript. Discrepancies between the data presented in the previous manuscript version and Young et al. (2019) are due to different data processing methods. In our case, we first applied the  $0.005 \text{ L}^{-1}$  threshold to our dataset and then interpolated ICNCs to the time resolution of temperature measurements. Young et al. (2019) interpolated ICNCs first and then applied the cut-off ICNC threshold. Their interpolation resulted sometimes in lower values, as interpolation between non-ice containing and ice containing regions occurred. The minimum value in their data however is  $0.007 \text{ L}^{-1}$ , still higher than the applied threshold. In other words applying even lower thresholds would not impact observational statistics. Nevertheless, for consistency between the two papers we now use the exact same data-processing method as in Young et al. (2019) and describe this in lines 242-244.

As far as modeled ICNCs are concerned, ice processes are calculated only if meaningful ice content is present ( $Q_i > 10^{-8} \text{ kg kg}^{-1}$ ). The minimum ICNC (sizes  $> 80 \mu\text{m}$ ) corresponding to these  $Q_i$  conditions found in the CNTRL model dataset is  $0.0008 \text{ L}^{-1}$ . This means that no meaningful ice is produced for INPs  $\sim 0.00005 \text{ L}^{-1}$ , which corresponds to supercooled liquid-only conditions in the model. Considering the high frequency of liquid-only clouds in the region, this is the expected behaviour.

### Supporting Information

Text S4: The statement here about the uncertainty in the parameterization used is correct, unlike the inference in the main manuscript. But again here, the 0.005 per liter threshold is mentioned in how it impacts the results of decreasing primary ice nucleation. Does this threshold need to exist? Again, it needs explanation, somewhere in this paper.

Yes, this threshold separates ice patches from liquid-only regions of the cloud. This is now stated in lines 243-244. Including non-ice containing clouds in the calculation of ice microphysical properties would cause a significant bias in the results.

**Figure S1 and others:** Is there a real reason why the scale needs to change? I was quite confused by these figures until I read the last statement of each caption.

Supplementary Figures have been moved to the main text (Figure 5 and 6). The same scaling is now used in all plots to avoid confusion.

### Reference:

Young, K. C., 1974: The Role of Contact Nucleation in Ice Phase Initiation in Clouds. *J. Atmos. Sci.*, **31**, 768–776, [https://doi.org/10.1175/1520-0469\(1974\)031<0768:TROCNI>2.0.CO;2](https://doi.org/10.1175/1520-0469(1974)031<0768:TROCNI>2.0.CO;2).

Young, G., Connolly, P. J., Jones, H. M., and Choulaton, T. W.: Microphysical sensitivity of coupled springtime Arctic stratocumulus to modelled primary ice over the ice pack, marginal ice, and ocean, *Atmos. Chem. Phys.*, **17**, 4209–4227, <https://doi.org/10.5194/acp-17-4209-2017>, 2017.

**Secondary ice production in summer clouds over the Antarctic coast:  
an underappreciated process in atmospheric models**

5 Georgia Sotiropoulou<sup>1,2</sup>, Étienne Vignon<sup>3</sup>, Gillian Young<sup>4</sup>, Hugh Morrison<sup>5,6</sup>, Sebastian J.  
O'Shea<sup>7</sup>, Thomas Lachlan-Cope<sup>8</sup>, Alexis Berne<sup>3</sup>, Athanasios Nenes<sup>1,9</sup>

<sup>1</sup>Laboratory of Atmospheric Processes and their Impacts (LAPI), Ecole Polytechnique  
Fédérale de Lausanne (EPFL), Lausanne, Switzerland

10 <sup>2</sup>Department of Meteorology, Stockholm University & Bolin Center for Climate Research,  
Sweden

<sup>3</sup>Environmental Remote Sensing Laboratory (LTE), EPFL, Lausanne, Switzerland

<sup>4</sup>School of Earth and Environment, University of Leeds, UK

<sup>5</sup>National Center for Atmospheric Research, Boulder, CO, USA

15 <sup>6</sup>ARC Centre for Excellence in Climate System Science, University of New South Wales,  
Sydney, Australia

<sup>7</sup>Centre for Atmospheric Science, University of Manchester, UK

<sup>8</sup>British Antarctic Survey, Cambridge, UK

<sup>9</sup>ICE-HT, Foundation for Research and Technology Hellas (FORTH), Patras, Greece

20 *Correspondence to:* georgia.sotiropoulou@epfl.ch, athanasios.nenes@epfl.ch

**Abstract**

The correct representation of Antarctic clouds in atmospheric models is crucial for accurate  
projections of the future Antarctic climate. This is particularly true for summer clouds which  
25 play a critical role in the surface melting of the ice-shelves in the vicinity of Weddell Sea. The  
pristine atmosphere over the Antarctic coast is characterized by low concentrations of Ice  
Nucleating Particles (INPs), which often result in the formation of supercooled liquid clouds.  
However, when ice formation occurs, the ice crystal number concentrations (ICNCs) are  
substantially higher than those predicted by existing primary ice nucleation parameterizations.  
30 The rime-splintering mechanism, thought to be the dominant secondary ice production (SIP)  
mechanism at temperatures between -8 and -3°C, is also weak in the Weather and Research  
Forecasting model. Including a parameterization for SIP due to break-up (BR) from collisions  
between ice particles improves ICNC representation in the modeled mixed-phase clouds,  
suggesting that BR could account for the enhanced ICNCs often found in Antarctic clouds.

35 The model results indicate that a minimum concentration of about  $0.1 \text{ L}^{-1}$  primary ice crystals is sufficient to initiate significant break-up, while there is little sensitivity to increasing INPs.

The BR mechanism is currently not represented in most weather prediction and climate models; including this process can have a significant impact on the Antarctic radiation budget.

#### 40 **1. Introduction**

Predictions of Antarctic climate are hampered by the poor representation of mixed-phase clouds over the Southern Ocean and the Antarctic Seas (Haynes et al., 2011; Flato et al., 2013; Bodas-Salcedo et al., 2014; Hyder et al., 2018). Model simulations reveal significant discrepancies in the Antarctic surface radiation budget, associated with cloud biases that are  
45 driven by errors in the representation of the cloud microphysical structure (Lawson and Gettelman, 2014; King et al., 2015; Listowski and Lachlan-Cope, 2017). A correct representation of the cloud radiative impacts largely depends on the parameterization of cloud microphysical processes (Listowski and Lachlan-Cope, 2017; Hines et al., 2019; Young et al., 2019) and precipitation (Vignon et al., 2019), which determine the concentration and  
50 characteristics of liquid drops and ice crystals.

Ice crystals form at temperatures above  $-38^{\circ}\text{C}$  through heterogeneous nucleation (Pruppacher and Klett, 1997); this means that the presence of insoluble aerosols that act as ice  
nucleating particles (INPs) is required. However, Antarctica and Southern Ocean are relatively clean regions and INPs are sparse (McCluskey et al., 2018; Schmale et al., 2019;  
55 Welti et al., 2020). Thus it is especially surprising that enhanced ice crystal number concentrations (ICNCs) have been observed in Antarctic clouds (Lachlan-Cope et al., 2016; O'Shea et al., 2017). Secondary ice processes are believed to magnify ICNCs in polar clouds with important implications for the surface radiative balance (Young et al., 2019), yet the underlying mechanisms remain highly uncertain (Field et al., 2017).

60 The only well-established SIP mechanism that has been extensively implemented in weather forecast and climate models is rime-splintering (Hallett and Mossop, 1974), also known as the Hallett-Mossop process (H-M), which refers to the production of ice splinters after collisions of supercooled droplets with ice particles (Hallett and Mossop, 1974; Heymsfield and Mossop, 1984). This process is effective only in a limited temperature range,  
65 between  $-8$  and  $-3^{\circ}\text{C}$ , and requires the presence of supercooled liquid droplets both smaller and larger than  $13 \mu\text{m}$  and  $24 \mu\text{m}$ , respectively (Mossop and Hallett, 1974; Choulaton et al., 1980). However, recent studies have shown that H-M cannot sufficiently explain the

enhanced ICNCs observed in both Arctic (Sotiropoulou et al., 2020) and Antarctic (Young et al., 2019) clouds. While some Antarctic studies (Vergara-Temprado et al., 2018; Young et al., 2019) suggest that the underestimation of ice multiplication in models might be related to uncertainties in the description of the H-M process, we argue that this is likely driven by the fact that almost no models include other SIP mechanisms.

Another SIP mechanism, identified in recent laboratory studies (Leisner et al., 2014; Lauber et al., 2018), is the generation of ice fragments from shattering of relatively large frozen drops. This process however, while very efficient in convective clouds (Korolev et al., 2019), has been found ineffective in polar regions (Fu et al., 2019; Sotiropoulou et al., 2020). This is in agreement with Lawson et al. (2017) and Sullivan et al. (2018a) who have shown that drop-shattering occurs in clouds with a relatively warm cloud base.

Mechanical break-up (BR) of ice particles that collide with each other is another process that results in ice multiplication (Vardiman, 1978; Takahashi et al., 1995) and it operates over a wide temperature range with maximum efficiency around  $-15^{\circ}\text{C}$ . Limited knowledge of the BR mechanism comes from few laboratory experiments (Vardiman, 1978; Takahashi et al., 1995) and small-scale modeling (Fridlind et al., 2007; Yano and Phillips, 2011, 2016; Phillips et al., 2017a,b; Sullivan et al., 2018a; Sotiropoulou et al., 2020). To the authors knowledge only two attempts have been made to incorporate this process in mesoscale models (Sullivan et al., 2018b; Hoarau et al., 2018). Specifically, Hoarau et al. (2018) assumed a constant number of fragments ( $F_{BR}$ ) generated per snow-graupel collision in Meso-NH model, while Sullivan et al. (2018b) implemented a temperature-dependent relationship for  $F_{BR}$  in COSMO-ART for several types of collisions (e.g. crystal-graupel, graupel-hail, etc), based on the results of Takahashi et al. (1995). Phillips et al. (2017a) recently developed a physically-based description of  $F_{BR}$ , which is a function of collisional kinetic energy and accounts for the effect of the colliding particles' size and rimed fraction ( $\Psi$ ). While being more advanced than any other parameterization proposed for BR, this scheme has never been implemented in mesoscale models before; it has only been tested in small-scale models for convective clouds (Phillips et al., 2017b; Qu et al., 2020) and Arctic stratocumulus (Sotiropoulou et al., 2020).

Sotiropoulou et al. (2020) recently showed that the observed ICNCs in Arctic clouds within the H-M temperature zone can be explained only by the combination of BR with the H-M process, which results in a 10 to 20-fold enhancement of the primary ice crystals. Based on their results, we postulate that BR may also play a critical role in Antarctic clouds and can potentially explain the discrepancy between the observed and modeled ICNCs in the region

(Young et al., 2019). To test this hypothesis, we implement parameterizations of the BR process in the Morrison microphysics scheme (Morrison et al., 2005) (hereafter M05) in the Weather and Research Forecasting (WRF) model V4.0.1 and examine their influence on the Antarctic clouds observed during the Microphysics of Antarctic Clouds (MAC) field campaign (O’Shea et al., 2017; Young et al., 2019).

## 2. Observations

### 110 2.1. MAC Instrumentation

The MAC field campaign was conducted in November–December 2015 over coastal Antarctica and the Weddell Sea, with the aim to offer detailed measurements of the microphysical and aerosol properties of the coastal Antarctic atmosphere. MAC included an extensive suite of airborne and ground-based instruments, a detailed description of which can be found in O’Shea et al. (2017). Here we only offer a brief recap of the instrumentation used in this study.

Cloud particle size distributions were derived using the images from a 2D Stereo (2DS, SPEC Inc., USA; Lawson et al., 2006) probe with a nominal size range from 10 to 1280  $\mu\text{m}$  (10  $\mu\text{m}$  pixel resolution). Shattering effects at the probes’ inlet were corrected by applying “antishatter” tips (Korolev et al., 2011) and inter-arrival time (IAT) post analysis (Crosier et al., 2011). The 2DS is a single particle instrument, measuring all particles that pass through its sample volume, which depends on particle size and the data integration period. For example, at 300  $\mu\text{m}$ , 1 count measured using over a 1-sec averaging window equals to a concentration of 0.27  $\text{L}^{-1}$ ; the uncertainty due to counting statistics is 100%. Total uncertainty is even higher but cannot be quantified.

Aerosol particle measurements of sizes 0.25 to 32  $\mu\text{m}$  were made using the Grimm optical particle counter (GRIMM model 1.109), while a Cloud Aerosol Spectrometer (CAS, DMT; Baumgardner et al., 2001; Glen and Brooks, 2013) measured particles between 0.6 to 50  $\mu\text{m}$ . Following the methodology of Young et al. (2019) and O’Shea et al. (2017), we only consider Grimm measurements of particles with diameter smaller than 1.6  $\mu\text{m}$  in our analysis to avoid including data subject to inlet losses at larger particle sizes. Finally, the aircraft also included instrumentation to measure temperature, turbulence, humidity, radiation and surface temperature (King et al., 2008).

### 135 2.2 Case study



For our investigations we focus on the MAC case examined in Young et al. (2019), for which they showed that the H-M process, as currently parameterized in WRF, cannot explain the observed ICNCs. Young et al. (2019) utilized measurements from two MAC flights, M218 and M219, combined in one case study; both flights were conducted on 27 November 2015 over the Weddell Sea (Fig. 1): M218 between 15.3-16.7 UTC and M219 between 20.45-22.5 UTC. On that day, a low pressure system persisted over the eastern Weddell Sea, resulting in a southeasterly flow reaching the aircraft with air mass back trajectories from around the low pressure system, towards the Antarctic Peninsula and southern Patagonia (O'Shea et al., 2017).

The temperature and microphysical conditions encountered during these flights are representative of the MAC campaign (see Table 1 in O'Shea et al., 2017, and Fig. S6 in Young et al., 2019). Cloud measurements were collected mainly within the lowest 1.1 km above sea-level (a.s.l.) during both flights and within a temperature range of  $\sim -9$  to  $-3^\circ\text{C}$ . The sampled stratocumulus clouds were dominated by supercooled liquid drops, while ice formation occurred in isolated ice patches characterized by substantially enhanced ICNCs; the mean (max) ICNCs in these cloud regions were  $1.16$  ( $9.03$ )  $\text{L}^{-1}$  and  $3.33$  ( $87.31$ )  $\text{L}^{-1}$  for M218 and M219, respectively. The mean concentration of aerosols with sizes between  $0.5$ - $1.6 \mu\text{m}$  was  $0.56 \text{ cm}^{-3}$  and  $0.41 \text{ cm}^{-3}$  ( $\text{cm}^{-3}$  at standard temperature and pressure) for the two flights. Such low aerosol conditions and concurrent high ICNC concentrations within this temperature range are frequently found in West Antarctic Peninsula (Lachlan-Cope et al., 2016). Moreover, similar cloud droplet concentrations ( $N_{drop}$ ) were measured during both flights (Young et al., 2019): the mean  $N_{drop}$  was  $82.7 \text{ cm}^{-3}$  for M218 and  $100.4 \text{ cm}^{-3}$  for M219, which are comparable with previous observations from the Antarctic Peninsula (Lachlan-Cope et al., 2016).

160

### 3. Modeling Methods

#### 3.1. Model set-up

This study is conducted with the WRF model (Skamarock et al., 2008), version 4.0.1, by applying the same model set-up as in Young et al. (2019). Two domains with a respective horizontal resolution of 5 km and 1 km are used, where the inner one is two-way nested to the parent domain (Fig. 1). The polar stereographic projection is applied. The outer domain is centered at  $74.2^\circ\text{N}$ ,  $30^\circ\text{E}$  and includes  $201 \times 201$  grid points, while the second domain consists of  $326 \times 406$  grids. Both domains have a high vertical resolution with 70 eta levels,

170 25 of which correspond to lowest 2 km of the atmosphere. The model top is set to 50 hPa. The  
simulation period spans from 26 to 28 November 2014, 00:00 UTC, allowing for a 24-hour  
spin up period before the day of interest (27 November). The model timestep is set to 30 (6)  
sec for the outer (inner) domain, while output data are produced every 30 minutes.

Input data for the initial, lateral and boundary conditions for the simulations are  
175 obtained from the European Centre for Medium-Range Weather Forecasting reanalysis (Dee  
et al., 2011), as recommended by Bromwich et al. (2013). For both shortwave and longwave  
radiation components, the RRTMG radiation scheme (Rapid Radiative Transfer Model for  
GCMs) is applied. The Mellor-Yamada-Nakanishi-Niino (MYNN; Nakanishi and Niino,  
2006) 2.5-level closure planetary boundary layer (PBL) and surface options are also  
180 implemented, in combination with the Noah Land Surface Model (Noah LSM; Chen and  
Dudhia, 2001), which includes a simplified thermodynamic sea-ice model. Given the short  
run length, time-varying sea ice concentrations are not utilized. Young et al. (2019) used the  
Polar WRF V3.6.1 to represent fractional sea-ice, a capability not available in standard WRF  
V3.6. However, this option has been made available in the more recent V4.0.1 that we use in  
185 this study. Following Young et al. (2019), the sea-ice albedo is set to 0.82, with a default  
thickness of 3 m, and snow accumulation depth on sea ice is allowed to vary between 0.001 m  
and 1.0 m.

A so-called ‘cumulus parameterization’ for shallow-convection subgrid processes is  
not activated in both domains to ensure all cloud processes are represented by the grid-scale  
190 microphysics scheme. Note that 5 km is a general upper limit for a convection-resolving  
resolution (Klemp, 2006; Prein et al., 2015). Cloud microphysics are parameterized following  
Morrison et al. (2005), hereafter M05. M05 performs well in reproducing Antarctic clouds,  
resulting in improved representation of the liquid phase and thus the cloud radiative effects  
compared to less advanced microphysical schemes (Listowski and Lachlan-Cope, 2017;  
195 Hines et al., 2019). This bulk microphysics scheme predicts mixing ratios and number  
concentrations for cloud ice, rain, snow and graupel species. While the mass mixing ratio of  
cloud water is a prognostic variable,  $N_{drop}$  is constant parameter. The default value of the  
scheme is  $200 \text{ cm}^{-3}$ ; here  $N_{drop}$  is set to  $92 \text{ cm}^{-3}$ , which is the mean value of M218 and M219  
flight measurements (see Section 2.2).

200

### 3.2 Sensitivity Simulations

A detailed description of the ice formation processes in M05 and the implemented BR  
parameterizations is offered in Appendix A and B, respectively. We assume that collisions

that include at least one large particle (thus ice-snow, ice-graupel and graupel-snow, snow-  
205 snow and graupel-graupel) result in ice multiplication; contribution from collisions between  
small ice particles (cloud ice) are neglected. In addition to the control (CNTRL) simulation,  
which corresponds to the default set-up of M05 and accounts only for H-M, we perform seven  
sensitivity simulations with varying description of  $F_{BR}$ . We also perform an additional  
simulation as in CNTRL except with no H-M, and thus no SIP at all, which is referred as  
210 NOSIP in the text.

In two sensitivity simulations with active break-up we assume, as in Hoarau et al.  
(2018), a constant number of fragments generated per collision. This number is constrained  
by in-situ measurements from the Arctic (Schwarzenboeck et al., 2009) which indicated that  
one-branch ice-crystals are more common in polar clouds, resulting in ejection of a single  
215 fragment after collision with another ice particle. However, this analysis (Schwarzenboeck et  
al., 2009) included only dendritic crystals with size larger than 300  $\mu\text{m}$ . Based on these results  
we perform two simulations: FRAG1 assumes all collision types generate one fragment  
without any size restrictions, while FRAG1siz allows for ice multiplication only if the particle  
that undergoes fragmentation is larger than 300  $\mu\text{m}$ . Note that because cloud ice with  
220 characteristic diameter larger than 250  $\mu\text{m}$  is converted to snow in the M05 scheme, collisions  
that include cloud ice are assumed to not result in any multiplication in FRAG1siz.

The standard temperature-dependent formula of Takahashi et al. (1995) for  $F_{BR}$ ,  
applied in Sullivan et al. (2018b), is tested here in the TAKAH simulation. However,  
Takahashi et al. (1995) used 2-cm hailballs in their experiments, which is an unrealistic set-  
225 up. For this reason we perform an additional simulation, TAKAHsc, in which this relationship  
is further scaled with size (see Appendix B).

Finally, the Phillips parameterization is implemented in three simulations with varying  
 $\Psi$  for the cloud ice/snow particles that undergo fragmentation;  $\Psi$  is not predicted in most bulk  
microphysics scheme, including M05, and thus it is prescribed as a constant. Note that  $F_{BR}$  is  
230 a function of  $\Psi$  only for the ice crystals or snowflakes that undergo break-up, but not for  
graupel (Appendix B). Graupel is assumed to have  $\Psi \geq 0.5$ , while the other ice types are  
characterized by lower rimed fraction. For this reason, we will consider values of  $\Psi$  for cloud  
ice and snow between 0.2 (lightly rimed) and 0.4 (heavily rimed) (Phillips et al., 2017a, b).  
These simulations are referred as PHIL0.2, PHIL0.3 and PHIL0.4 in the text, where the  
235 number indicates the assumed values of  $\Psi$  of cloud ice and snow.

#### 4. Results

#### 4.1 BR effect on microphysical properties

In Fig. 2a the modeled total ice number concentrations (cloud ice + snow + graupel,  $N_{isg}$ )  
240 derived for the region encompassing the 2 MAC flights (Fig. 1) are compared with  
measurements derived from the 2D Stereo (2DS) probe (see Section 2.1 for details). ICNCs in  
Fig. 2 are interpolated to match the time resolution of the temperature measurements. Then  
cloud ice statistics are calculated for  $N_{isg} > 0.005 \text{ L}^{-1}$ , an indicator for the presence of an ice  
245 patch (O'Shea et al., 2017; Young et al., 2019). Moreover, since 2DS cannot resolve the  
shape (thus cloud phase) of particles smaller than  $80 \mu\text{m}$ , only modeled ice particles with  
sizes larger than this threshold are considered in Fig. 2, like in Young et al. (2019). While  
mean and maximum statistics are discussed below, additional statistical metrics (e.g. median  
and interquartile range) are shown in Fig. S1 (Text S1).

The mean observed  $N_{isg}$  for the whole MAC campaign generally fluctuates between  
250  $0.5\text{--}4.5 \text{ L}^{-1}$ . The variation in  $N_{isg}$  with temperature is somewhat larger for our case study  
(November 27), as maximum mean concentration goes up to  $\sim 6.4 \text{ L}^{-1}$  at  $T = -6.5^\circ\text{C}$ .  
Consistently lower concentrations are observed for temperatures  $\leq -7^\circ\text{C}$ , but the temperature  
statistics are poor for this temperature range as very few observations are available (Fig. 2a).  
The CNTRL simulation consistently underestimates the mean observations, producing mean  
255  $N_{isg} \sim 0.1 \text{ L}^{-1}$  over the examined temperature range (Fig. 2a). NOSIP produces similar results  
to CNTRL, suggesting that the H-M process included in default M05 (CNTRL) is hardly  
effective at all.

PHIL0.2 and PHIL0.3 also produce similar mean ICNCs to CNTRL (Fig. 2a, b),  
suggesting that lightly to moderately rimed ice particles do not contribute to ice multiplication  
260 through collisional break-up. The higher rimed fraction in PHIL0.4 results in very good  
agreement with mean observations (Fig. 2a), especially over the whole MAC campaign  
FRAG1siz also agrees well with mean observations, but when the size restrictions are ignored  
(FRAG1) the model gives substantial ICNC overestimation. TAKAH simulation also  
produces unrealistically high mean  $N_{isg}$ , while TAKAHsc is in closer agreement with  
265 observations. The largest deviations from observations for TAKAHsc are observed for  
temperatures below  $-7^\circ\text{C}$ , where no good measurement statistics are available (see discussion  
above).

Overall, CNTRL, PHIL0.2 and PHIL0.3 cannot reproduce the observed spectrum (Fig.  
2b) and substantially underestimate the frequency of ICNCs larger than  $1 \text{ L}^{-1}$ . PHIL0.4,  
270 FRAG1siz and TAKAHsc, however, can successfully reproduce the observed range of values  
(Fig. 2b), but the relative frequency remains somewhat underestimated. FRAG1 is in closest

agreement with the observed spectrum, while TAKAH often overestimates the relative frequency (Fig. 2b). Maximum ICNCs in FRAG1 and TAKAH are 6403 and 2600 L<sup>-1</sup>, respectively, which are about 70 and 30 times larger than the observed maximum value: 88 L<sup>-1</sup>. This suggests that BR parameterizations that do not account for the impact of size are rather unrealistic. The maximum ICNCs in PHIL0.4, FRAG1siz and TAKAHsc are 174 L<sup>-1</sup>, 150 L<sup>-1</sup> and 173 L<sup>-1</sup>, which agree to within a factor of two with observations, while they are substantially underestimated in CNTRL (7.8 L<sup>-1</sup>), PHIL0.2 (4.7 L<sup>-1</sup>) and PHIL0.3 (5.2 L<sup>-1</sup>).

Vertical distributions of cloud ice ( $N_i$ ), graupel ( $N_g$ ), snow ( $N_s$ ) and total ICNC ( $N_{isg}$ ) number concentration are examined in Fig. 3(a-d) for all simulations except those that produce unrealistically large concentrations (FRAG1 and TAKAH). The observed ICNCs are also shown in Fig. 3a and 3c. For consistency with M05, which converts all cloud ice particles with characteristic diameters larger than 250  $\mu\text{m}$  to snow, the same threshold is adopted for splitting the observational dataset in these two ice categories. Graupel concentrations cannot be distinguished in the measurements; however, the model simulations that are in better agreement with observations (Fig. 2) suggest that these are negligible compared to cloud ice/snow concentrations. Graupel concentrations in Fig. 3b are shown for the whole size spectrum. In contrast, cloud ice (Fig. 3a), snow (Fig. 3c) and total ICNCs (Fig. 3d) include only particles with size larger than 80  $\mu\text{m}$  for consistency with the observations shown in the same panel.

PHIL0.2 and PHIL0.3 produce slightly larger  $N_i$  (Fig. 3a) than CNTRL, but reduced  $N_g$  (Fig. 3b) values and similar or reduced  $N_s$  (Fig. 3c); these mean  $N_i$  and  $N_s$  profiles are orders of magnitude lower than the observed values. PHIL0.4, FRAG1siz and TAKAHsc produce similar  $N_i$  to the observations (Fig. 3a), while  $N_s$  is slightly underestimated (Fig. 3c). FRAG1siz is in somewhat better agreement with  $N_i$  observations than the other two simulations, especially at heights above 750 m a.s.l (Fig. 3a); this is also reflected in total ICNCs (Fig. 3d). Activating BR generally results in reduction of  $N_g$  (Fig. 3b). This decrease is larger than one order of magnitude in the three best performing simulations, compared to CNTRL, however we cannot assess which of these graupel profiles better represents reality. Nevertheless, we can overall conclude that PHIL0.4, FRAG1siz and TAKAHsc result in improved agreement of the vertical distribution of total ICNCs with observations compared to the rest of the simulations (Fig. 3d), including the default set-up of M05. Moreover, cloud ice concentrations (Fig. 3a) are comparable to snow concentrations (Fig. 3c) in these three simulations, in agreement with observations. In contrast, simulations with deactivated or negligible BR result in substantially larger number of snow than cloud ice particles. This

indicates that BR shifts the ice particle spectra to smaller sizes, which results in a more realistic representation of the ice microphysical characteristics.

310 The simulated liquid water content (LWC) is compared with CAS observations in Fig. 4. All simulations, except TAKAH, produce similar or slightly overestimated mean LWC at temperatures  $\leq -3.5^{\circ}\text{C}$ ; at  $-3^{\circ}\text{C}$  the mean observed values are higher (Fig. 4a). An overestimation of LWC in these runs is more evident in Fig. 4b; the observed spectrum does not include values larger than  $0.5\text{ g m}^{-2}$ , while the simulated spectra are wider. An exception to this is TAKAH simulation, which underestimates mean LWCs and glaciates clouds at temperatures below  $-7^{\circ}\text{C}$  (Fig. 4a), while it produces a narrower LWC spectrum compared to the observed (Fig. 4b). Apart from TAKAH, the remaining simulations produce similar liquid water properties with minor improvements in the runs with reduced LWC values, e.g. in FRAG1 (Fig. 4a). Nevertheless, while the produced range of LWC values in FRAG1 is somewhat closer to the observed, it still underestimates the relative frequency for most of the observed spectrum (Fig. 4b).

320

#### 4.2 BR effect on surface radiation

To examine how deviations in ICNCs affect climate, mean radiative fluxes at the surface and at the top of the atmosphere (TOA) for all model simulations are presented in Table 1. Note that mass mixing ratio fields for all cloud species are provided from the microphysics to the radiation scheme, but no information on droplet and ice effective radius is exchanged.

325

Increasing BR multiplication has a pronounced impact on shortwave radiation, as it results in decreasing sunlight reflection and thus increasing downward surface radiation ( $\text{SWD}_{\text{SFC}}$ ). Upward surface radiation ( $\text{SWU}_{\text{SFC}}$ ) is a function of SWD and thus exhibits similar behaviour. This is due to the fact that increased BR efficiency (Fig. 2) results in decreased liquid water path (LWP) and cloud albedo. The difference between CNTRL and the simulations that improve ICNC representation (PHIL0.4, FRAG1siz and TAKAHsc) fluctuates between  $11.9\text{-}25.7\text{ W m}^{-2}$  for  $\text{SWD}_{\text{SFC}}$  and  $6.7\text{-}12.4\text{ W m}^{-2}$  for  $\text{SWU}_{\text{SFC}}$  (Table 1).

330

Cloud longwave radiative effects are mainly determined by cloud liquid properties, since liquid water is more opaque to longwave radiation than ice particles. However, no substantial differences in mean LWP are indicated for CNTRL ( $40.1\text{ g m}^{-2}$ ), PHIL0.2 ( $33.2\text{ g m}^{-2}$ ), PHIL0.3 ( $40.2\text{ g m}^{-2}$ ), PHIL0.4 ( $29.1\text{ g m}^{-2}$ ) and FRAG1siz ( $30.1\text{ g m}^{-2}$ ), since LWP values fall within the black body emission range (Stephens, 1978). Optically thinner clouds are produced in TAKAHsc ( $23.1\text{ g m}^{-2}$ ), and especially in FRAG1 ( $8.2\text{ g m}^{-2}$ ) and TAKAH ( $3.2\text{ g m}^{-2}$ ) runs. Note that most simulations, including CNTRL, produce wider LWC spectra

335



340 than the observed, by overestimating cloud liquid (Fig. 4b). Generally, decreasing liquid  
content is in better agreement with observations (see section 4.1), suggesting that including  
the BR process in M05 likely shifts the simulated LWPs towards more realistic values.  
However, excessive ice multiplication, as in TAKAH, results in unrealistic liquid properties  
(Fig. 4a) and thus errors in surface radiation.

345 Pronounced reduction in ( $LWD_{SFC}$ ) is only found for the simulations FRAG1siz,  
FRAG1 and TAKAHsc, which have a mean LWP well below  $30 \text{ g m}^{-2}$ , the lowest limit of the  
black body emission range (Stephens, 1978). In all other simulations, the reduction in cloud  
liquid due to BR is not large enough to alter the cloud emissivity significantly. The upward  
longwave component ( $LWU_{SFC}$ ) is only slightly affected in all simulations ( $< \sim 1.3 \text{ W m}^{-2}$ ).  
350 Young et al. (2019) showed that underestimation of ICNCs results in significant positive and  
negative biases in the surface Cloud Radiative Forcing (CRF) over the coastal areas; our  
results agree with their findings, as CRF biases vary between  $-78 \text{ W m}^{-2}$  and  $+86 \text{ W m}^{-2}$  for  
the most realistic simulations (Fig. S2, Text S2). Furthermore, the difference between  
CNTRL and the realistic simulations in upward radiation flux at TOA (Table 1) is also more  
355 pronounced for the shortwave component ( $SWU_{TOA}$ ), fluctuating between  $4.7\text{-}9.2 \text{ W m}^{-2}$ , and  
less significant for  $LWU_{TOA}$  ( $1.4\text{-}3.6 \text{ W m}^{-2}$ ). Ultimately, both surface and TOA radiation  
results indicate that a correct representation of SIP in the atmospheric models is critical for  
the projection of the energy budget and thus for the future Antarctic climate.

#### 360 **4.3 Sensitivity to uncertainties in H-M description**

To investigate the interactions between BR and H-M, we compare simulations in which the  
H-M efficiency is either enhanced or turned off. Young et al. (2019) remove all liquid  
thresholds from the H-M description, allowing for the process to become active over the  
whole droplet spectrum. However, this change resulted in very weak ICNC enhancement in  
365 their simulations. Here, we further remove all graupel/snow thresholds from H-M description  
(Appendix A), which implies that there no size restrictions for the initiation of the process.  
This modification is applied to CNTRL, PHIL0.3 and PHIL0.4 set-up, resulting in three  
additional sensitivity tests: CNTRL\_NOTHRES, PHIL0.3\_NOTHRES and  
PHIL0.4\_NOTHRES, respectively. Furthermore, in addition to NOSIP which corresponds to  
370 CNTRL set-up but without H-M, another two simulations are performed with BR active but  
H-M completely deactivated: PHIL0.3\_NOHM and PHIL0.4\_NOHM.

Mean ICNCs in CNTRL\_NOTHRES are enhanced by on average a factor of three  
compared to CNTRL (Fig. 5a). However this simulation underestimates concentrations at

Georgia 7/8/2020 13:09

**Comment [1]:** Section moved from SI to  
main text. New sensitivity tests with no liquid  
and ice thresholds in HM

375 temperatures larger than  $-7^{\circ}\text{C}$ : the mean observed value at this range is  $2\text{ L}^{-1}$ , while the  
simulated mean is  $0.3\text{ L}^{-1}$ . Good agreement between CNTRL\_NOTHRES and observations is  
only achieved at temperatures  $< -7^{\circ}\text{C}$ , where statistical metrics for the two MAC cases are  
poor (see Section 4.1). While PHIL0.3 did not result in any substantial multiplication, mean  
ICNCs in PHIL0.3\_NOTHRES are 5 times larger. The difference between PHIL0.4 and  
380 PHIL0.4\_NOTHRES is generally small for temperature warmer than  $-7^{\circ}\text{C}$ , not exceeding a  
factor of two, but it becomes substantially larger at colder temperatures. However, while the  
95<sup>th</sup> percentiles for CNTRL\_NOTHRES and PHIL0.3\_NOTHRES are similar and more  
comparable to observations, mean percentiles in PHIL0.4\_NOTHRES produces values larger  
than  $10\text{ L}^{-1}$  at all temperatures considered (Fig. 5b).

Excluding the temperature range ( $< -7^{\circ}\text{C}$ ) that does not include substantial number of  
385 measurements to evaluate model results, mean ICNC observations generally lay between  
PHIL0.3\_NOTHRES and PHIL0.4\_NOTHRES in this set of simulations, while  
CNTRL\_NOTHRES produces somewhat lower values (Fig. 5a). However, this set-up likely  
overestimates H-M efficiency, as it doesn't include any size limitations, which is not  
consistent with current knowledge on the H-M mechanism derived from laboratory studies  
390 (Hallet and Mossop, 1974; Choulaton et al., 1980). Nevertheless, the adapted thresholds are  
ad-hoc, tuned for different conditions; these should be refined to get a more realistic H-M  
effect in polar clouds.

Deactivating H-M completely does not substantially impact the results. This further  
confirms the fact that the prescribed ad-hoc thresholds prevent the initiation of the process in  
395 the studied conditions. Furthermore, it indicates that BR mechanism can explain the observed  
ICNCs independently of whether H-M is active or not.

#### 4.4 Sensitivity to uncertainties in primary ice formation

None of the utilized primary ice nucleation parameterizations are calibrated for the pristine  
400 conditions encountered over the high-latitude Southern Ocean, thus it is likely that primary  
ice formation is overestimated in this case. Moreover, recent studies have suggested the  
important role of bioaerosols as INPs at the examined relatively warm temperatures (DeMott  
et al., 2016); this INP type is not accounted for in existing ice nucleating particle  
parameterizations. To examine how the uncertainty in parameterizations for primary ice  
405 affects SIP efficiency, we perform two sets of simulations by dividing or multiplying the  
efficiency of all primary ice production mechanisms (immersion freezing, contact freezing  
and deposition/condensation-freezing nucleation) by a factor of 10. Specifically, the first set

with diminished ice nucleation includes CNTRL\_INP0.1, PHIL0.3\_INP0.1 and PHIL0.4\_INP0.1, while the second set with enhanced nucleation consists of CNTRL\_INP10, PHIL0.3\_INP10 and PHIL0.4\_INP10.

Decreasing primary ice production by a factor of 10 inhibits BR multiplication (Fig. 6). Note that while maximum  $N_{isg}$  in PHIL0.3\_INP0.1 and PHIL0.4\_INP0.1 is  $8.8 \text{ L}^{-1}$  and  $11 \text{ L}^{-1}$  respectively, these simulations produce lower mean values (Fig. 6a) and  $N_{isg95}$  (Fig. 6b) than CNTRL\_INP0.1 with maximum  $N_{isg}$   $5.7 \text{ L}^{-1}$ . This is partly because a larger number of values in CNTRL\_INP0.1 fall below the  $0.005 \text{ L}^{-1}$  threshold and are not included in the presented mean statistics. Nevertheless, it is clear that the fewer primary ice crystals in all these sensitivity tests result in decreased frequency of ice-ice particle collisions, which is not sufficient to initiate significant BR multiplication.

Increasing primary ice production by an order of magnitude in CNTRL\_INP10 still results in underestimated ice concentrations than observed, providing additional evidence for the significant role of SIP in these conditions. The increased concentration of primary ice crystals enhances BR efficiency in PHIL0.3\_INP10 compared to PHIL0.3, however the produced mean concentrations still are lower than the observed;  $N_{isg95}$  in PHIL0.3\_INP10 only slightly exceeds unity (Fig. 6b). In contrast, PHIL0.4\_INP10 produces similar mean ICNCs with PHIL0.4.  $N_{isg95}$  is also similar at warmer temperatures between two simulations, while larger deviations are observed at temperatures  $\leq -7^\circ\text{C}$  (Fig. 6b). This suggests that increasing concentrations of available ice particles tend to decrease the efficiency of BR mechanism, hence possible overestimations in primary ice production are likely offset by decreasing production of secondary ice.

In summary, the above results indicate that BR cannot be initiated when the available primary ice concentrations are substantially lower than  $0.1 \text{ L}^{-1}$ , which is the mean primary ICNCs produced in NOSIP simulation (Fig. 2a). Yet, INPs over Southern Ocean are often substantially lower (McCluskey et al., 2018; Schmale et al., 2019; Welti et al., 2020). Ice seeding from clouds above the boundary layer was suggested by Young et al. (2019) as a key contributor to the primary ICNC levels for the studied case (see their Supporting Information). Another process that can likely result in optimal conditions for BR to be initiated is aerosol transport from the Antarctic continent, where terrestrial INPs are higher (Vergara-Temprado et al., 2018). Moreover, a combination of these processes and the H-M mechanism, whose efficiency is substantially restricted in the current version of M05, might also provide the necessary concentrations to initiate BR; this was also the case for Arctic stratocumulus conditions in Sotiropoulou et al. (2020). Understanding these interactions

between different processes in the Antarctic region would likely provide insights to the conditions that favor the development of isolated ice patches with substantially high ICNCs within predominantly supercooled liquid clouds. In higher INP conditions, which are likely less representative of the coastal Antarctic climate, the sensitivity of BR parameterization is expected to be lower.

## 5. Conclusions

Our results indicate that collisional break-up of ice crystals can explain observations of enhanced ICNCs in coastal Antarctic clouds, but this process requires the presence of  $\sim 0.1 \text{ L}^{-1}$  primary ice crystals (as produced in NOSIP simulation) for initiation. This likely is a key threshold that can lead the development of isolated ice patches with enhanced ICNCs in predominantly supercooled liquid clouds (Grosvenor et al., 2012; O'Shea et al., 2017). Over the Southern Ocean, when INPs are generally sparse (McCluskey et al., 2018; Schmale et al., 2019; Welti et al., 2020), such conditions could likely be achieved through ice seeding (as likely happens in the examined case) or through INP transport from the Antarctic continent, where INP concentrations are generally higher (Vergara-Temprado et al., 2018).

Although BR has been observed in polar conditions before (Rangno and Hobbs, 2001; Schwarzenboeck et al., 2009), this mechanism is currently not implemented in most weather prediction and climate models. The more advanced Phillips et al. (2017a) parameterization produces realistic ICNCs in Antarctic clouds as long as a high rimed fraction is prescribed for the particles that undergo fracture, in agreement with Sotiropoulou et al. (2020). This indicates that our conclusions may not hold for winter clouds in the region, which contain less supercooled liquid water (Listowski et al., 2019) and are less prone to riming. However, for the studied case, a comparison of vapor deposition rates with riming rates (which include mass changes due to collisions with droplets/raindrops and due to contact/immersion freezing) for CNTRL simulation indicate that these two are on average comparable for cloud ice, while riming rates are substantially larger than vapor deposition rates for snow (not shown). These results suggest that prescribing a high rimed fraction for cloud ice and snow in M05 is not unreasonable; nevertheless  $\Psi$  in reality is highly variable for different temperature and microphysical conditions. More simplified parameterizations also produce improved results as long as the impact of the dependence of  $F_{BR}$  on the ice particle size is accounted for.

The very few existing BR descriptions in mesoscale models either do not account for size limitations (Sullivan et al., 2018b) or do not account for all collision types (Hoarau et al., 2018), which limits their realism. Increasing ICNCs from BR alters significantly the radiative

effects of summer mixed-phase Antarctic clouds; these clouds play a critical role in the surface melting of ice-shelves in the vicinity of Weddell Sea (Gilbert et al., 2020) and thus their accurate microphysical representation in models is of great importance.

#### 480 **Appendix A: Ice formation processes in M05 scheme**

The standard M05 scheme includes three primary ice production mechanisms through heterogeneous nucleation (immersion freezing, contact freezing and deposition/condensation-freezing nucleation), and one SIP process (H-M).

Immersion freezing of cloud droplets and rain is based on the work of Bigg (1953).

485 This mechanism is active below  $-4^{\circ}\text{C}$  and produces a raindrop freezing rate that depends on the degree of supercooling and the number concentration and volume of supercooled drops. The Meyers et al. (1992) description is used for contact freezing, also active below  $-4^{\circ}\text{C}$ . The effective diffusivity of the contact nuclei to the drops are estimated from Brownian motion similar to Young (1974):  $D_{ap} = R T (6 p r_i N_A m)^{-1} [1 + 0.0737 T (2880P)^{-1} r_i^{-1}]$ , where  $R$  is the universal gas constant,  $N_A$  is Avogadro's number,  $m$  is the dynamic viscosity of air,  $T$  is the temperature,  $P$  is the air pressure, and the radius of ice nuclei  $r_i$  is assumed to be  $1 \times 10^{-7}$  m. 490 The factor in the brackets  $[\ ]$  is a correction factor accounting for the mean free path of air molecules relative to the size of the ice nuclei (all units are MKS).

The default parameterization for deposition/condensation-freezing ice nucleation in 495 M05 is from Cooper (1986), which depends only on temperature and is active below  $-8^{\circ}\text{C}$  in liquid saturated conditions or when ice supersaturation exceeds 8%. However, the aerosol-aware DeMott et al. (2010) parameterization for heterogeneous nucleation has been shown to compare better with in-cloud ice measurements over the Antarctic Peninsula than Cooper (Listowski and Lachlan-Cope, 2017), although none of these schemes is likely accurate as 500 they have been calibrated for less pristine conditions. Nevertheless, both Cooper and DeMott produce similar primary ice concentrations over the temperature range covered by the observations, but Cooper predicts more primary ice at lower temperatures ( $<13^{\circ}\text{C}$ ), which might affect the representation of higher-altitude clouds (see Supporting Information in Young et al. 2019). For this reason, we apply the DeMott description in our simulations, 505 where the mean aerosol concentration of particles with sizes between  $0.5\text{-}1.6 \mu\text{m}$  for the two flights ( $0.49 \text{ scm}^{-3}$ ) is used as input (Young et al., 2019). Uncertainty to this formulation is investigated through a number of sensitivity tests (section 4.4).

The H-M parameterization, adapted from Reisner et al. (1998), is based on the laboratory experiments conducted by Hallett and Mossop (1974), who found a maximum of

510 ~350 splinters per milligram of rime generated around  $-5^{\circ}\text{C}$ :

$$\frac{dN_{iHM}}{dt} = \rho \cdot 3.5 \cdot 10^8 f(T) \frac{dm_{rime}}{dt} \quad (1)$$

where  $dN_{iHM}/dt$  is the number of new fragments produced at a given timestep,  $f(T)$  is the temperature-dependent efficiency of the process,  $\rho$  is the air density, and  $dm_{rime}/dt$  is the mass production rate of rime on snow or graupel due to accretion of cloud and rain drops.  $f(T)$  is 0 for  $T < -8^{\circ}\text{C}$  and  $T > -3^{\circ}\text{C}$ , 1 for  $T = -5^{\circ}\text{C}$ , and increases linearly between these two extremes for  $T \geq -8^{\circ}\text{C}$  and  $T \leq -3^{\circ}\text{C}$ .

515 Furthermore, for H-M to become activated in M05, two conditions must be met: (a) snow (or graupel) mass mixing ratios must be greater than  $0.1 \text{ g kg}^{-1}$  and (b) cloud liquid (or rain) water mass mixing ratios should be greater than 0.5 (or 0.1)  $\text{g kg}^{-1}$ . To achieve a good agreement between modeled and observed ICNCs for the simulated case, Young et al. (2019) had to remove condition (b) and multiply the H-M efficiency by a factor of 10.

### Appendix B: Parameterizing collisional break-up in M05

525 There are three types of ice particles considered in the M05 scheme: small (cloud) ice, snow, and graupel. Ice multiplication is allowed after cloud ice-snow, cloud ice-graupel, graupel-snow, snow-snow and graupel-graupel collisions. The standard M05 scheme includes a description for collisions between cloud ice and snow to represent the accretion process, following the ‘‘continuous collection’’ approach:

$$\frac{dN_{iAC}}{dt} = \frac{\pi}{4} \rho E_{col} \Gamma(b_s + 3) a_s \frac{N_i N_{os}}{\lambda_s^{(b_s+3)}} \quad (2)$$

530  $dN_{iAC}/dt$  is the rate of ice crystal number concentration collected by snow.  $N_{os}$  and  $\lambda_s$  are the intercept and slope parameters of the snow size distribution, represented by an inverse exponential function, and  $\Gamma$  is the Euler gamma function.  $a_s$  and  $b_s$  are the characteristic parameters for snow in the fallspeed-diameter relationship (Morrison et al., 2005);  $a_s$  includes a density correction factor (Heymsfield et al., 2007). Note that the diameter ( $d_i$ ) and terminal velocity ( $u_i$ ) of cloud ice particles are considered much smaller than those of snow:  $d_i \ll d_s$  and  $u_i \ll u_s$ , so that they are neglected in Eq. (2).  $E_{col}$  is the collection (sticking) efficiency between ice particles, set to 0.1; hence, it is assumed that only 10% of cloud ice particles that collide with snow are actually collected. We assume the remaining 90% of collisions result in ice particle break-up, hence the following relationship gives the rate of cloud ice-snow collisions

540 that contribute to ice multiplication:

$$\frac{dN_{iis}}{dt} = \frac{\pi}{4} \rho (1 - E_{col}) \Gamma(b_s + 3) a_s \frac{N_i N_{os}}{\lambda_s^{(b_s+3)}} \quad (3)$$



In the default M05, collisions between cloud ice and graupel particles are neglected as it is assumed that the collection efficiency of such collisions is negligible. To represent cloud ice-graupel collisions for ice multiplication, we use Eq. (3), but the size distribution and fallspeed parameters of snow are replaced by those for graupel. Moreover, since cloud ice is not collected by graupel particles, we assume that 100% of these collisions result in cloud ice break-up:

$$\frac{dN_{ig}}{dt} = \frac{\pi}{4} \rho \Gamma (b_g + 3) a_g \frac{N_i N_{0g}}{\lambda_g^{b_g+3}} \quad (4)$$

In the default M05 scheme, collisions between snow and graupel are also neglected because it is assumed that the collection efficiency for such collisions is negligible. For this study, graupel-snow collisions are treated using expressions similar to those for raindrop-snow collisions in M05. These are adapted from Ikawa and Saito (1991) and represent collisions between relatively large precipitation-sized particles:

$$\frac{dQ_{isg}}{dt} = \pi^2 \rho_s \rho \left| \Delta u_{m_{sg}} \right| \frac{N_{0s} N_{0g}}{\lambda_s^3} \left( \frac{5}{\lambda_s^3 \lambda_g} + \frac{2}{\lambda_s^2 \lambda_g^2} + \frac{0.5}{\lambda_s \lambda_g^3} \right) \quad (5)$$

$$\frac{dN_{isg}}{dt} = \frac{\pi}{2} \rho \left| \Delta u_{n_{sg}} \right| N_{0s} N_{0g} \left( \frac{1}{\lambda_s^3 \lambda_g} + \frac{1}{\lambda_s^2 \lambda_g^2} + \frac{1}{\lambda_s \lambda_g^3} \right) \quad (6)$$

$$\text{where } \left| \Delta u_{m_{sg}} \right| = \left( (1.2u_{ms} - 0.95u_{mg})^2 + 0.08u_{mg}u_{ms} \right)^{1/2} \quad (7)$$

$$\text{and } \left| \Delta u_{n_{sg}} \right| = \left( (1.7u_{ns} - u_{ng})^2 + 0.3u_{ng}u_{ns} \right)^{1/2} \quad (8)$$

$dQ_{isg}/dt$  and  $dN_{isg}/dt$  represent the bulk rates that snow mass and number concentration collide with graupel and contribute to ice multiplication through fragmentation. Corrections in the mass (or number) -weighted difference in terminal velocity  $\Delta u_{m_{sg}}$  (or  $\Delta u_{n_{sg}}$ ) of the colliding particles (Eq. 7,8) are adapted from Mizuno (1990) and Reisner et al. (1998), to account for underestimates when  $u_{ns} \approx u_{ng}$ .

M05 also includes a description for collisions between snowflakes to represent snow aggregation, following Passarelli (1978):

$$\frac{dN_{sAg}}{dt} = \frac{-1108a_s E_{col}}{4 \times 720} \pi^{\frac{1-b_s}{3}} \rho^{\frac{2+b_s}{3}} \rho_s^{\frac{-2-b_s}{3}} Q_s^{\frac{2+b_s}{3}} N_s^{\frac{4-b_s}{3}} \quad (9)$$

Based on this expression we parameterize the number of snow-snow collisions that contribute to ice multiplication as:

$$\frac{dN_{iss}}{dt} = \frac{1108a_s(1-E_{col})}{4 \times 720} \pi^{\frac{1-b_s}{3}} \rho^{\frac{2+b_s}{3}} \rho_s^{\frac{-2-b_s}{3}} Q_s^{\frac{2+b_s}{3}} N_s^{\frac{4-b_s}{3}} \quad (10)$$

Because snow aggregation does not result in any mass transfer, the snow mass involved in these collisions is not calculated by the default M05 scheme. We obtain a description of  $dQ_{iss}$

/dt by applying the size distribution and fallspeed parameters of snow in the analytical solution for self-collection derived by Verlinde et al. (1990):

$$\frac{dQ_{i_{ss}}}{dt} = \frac{914\pi^2}{48\rho\rho_s} (1 - E_{col}) a_s d_s^{b_s+5} N_s^2 \quad (11)$$

To test the consistency of Eq. (10) and (11), which were derived using different methods, we repeated the CNTRL and PHIL0.4 simulations but with the Eq. (9) and (10) replaced by the analytical solution for the change in number concentration from self-collection derived by Verlinde and Cotton (1993). The sensitivity of the results to this modification was found to be insignificant.

Graupel-graupel collisions are also parameterized in a similar manner. Since there is no graupel aggregation (collection efficiency of such collisions is assumed to be negligible), 100% of the collisions are assumed to contribute to break-up:

$$\begin{aligned} \frac{dN_{i_{gg}}}{dt} &= \frac{1108a_g}{4 \times 720} \pi^{\frac{1-b_g}{3}} \rho^{\frac{2+b_g}{3}} \rho_g^{\frac{-2-b_g}{3}} Q_g^{\frac{2+b_g}{3}} N_g^{\frac{4-b_g}{3}} \quad (12) \\ \frac{dQ_{i_{gg}}}{dt} &= \frac{836\pi^2}{48\rho\rho_g} a_g d_g^{b_g+5} N_g^2 \quad (13) \end{aligned}$$

The value 1108 in Eq. (10) is valid for  $b_s=0.4$  (Passarelli, 1978); in M05  $b_s=0.41$  and  $b_g=0.37$ , thus adapting this value for both snow-snow (10) and graupel-graupel (12) collisions is a reasonable approximation.

Following the methodology of Sullivan et al. (2018b) in TAKAH simulation, the number of fragments generated due to ice-ice particle collisions ( $F_{BR}$ ) is:

$$F_{BR} = 280 (T - 252)^{1.2} e^{-(T-252)/5} \quad (14)$$

However, Takahashi et al. (1995) used 2-cm hailballs in their experiments, thus to further include the influence of size in this formulation, we implement a size-scaled expression in TAKAHsc simulation, assuming that  $F_{BR}$  depends linearly on  $D$ , decreasing to 0 at  $D = 0$ :

$$F_{BR} = 280 (T - 252)^{1.2} e^{-(T-252)/5} \frac{D}{D_o} \quad (15)$$

where  $D$  (in meters) is the size of the ice particle that undergoes fracturing and  $D_o=0.02$  m, the size of hailballs used by Takahashi et al. (1995).

The Phillips et al. (2017a) parameterization allows for varying treatment of  $F_{BR}$  depending on the ice crystal type and habit.

$$F_{BR} = \alpha A \left( 1 - \exp \left\{ - \left[ \frac{CK_o}{\alpha A} \right]^\psi \right\} \right) \quad (16)$$

$$\text{where : } K_o = \frac{m_1 m_2}{m_1 + m_2} (\Delta u_{n_{12}})^2,$$

$$\psi = 3.5 \times 10^{-3}$$

$$a = \pi D^2$$

600  $m_1, m_2$  are the masses of the colliding particles and  $\Delta u_{n12}$  is the difference in their terminal velocities. The correction applied in Eq. (8) is also adapted here to account for underestimates when  $u_{n1} \approx u_{n2}$ .  $D$  (in meters) is the size of the smaller ice particle which undergoes fracturing and  $\alpha$  is its surface area. The parameterization was developed based on particles with diameters  $500 \mu\text{m} < D < 5 \text{ mm}$ , however Phillips et al. (2017a) suggest that it can be  
 605 used for particle sizes outside the recommended range as long as the input variables to the scheme are set to the nearest limit of the range.  $C$  is the asperity-fragility coefficient and  $\psi$  is a correction term for the effects of sublimation based on the field observations by Vardiman (1978). For cloud ice-snow, cloud ice-graupel, snow-graupel and snow-snow collisions:

$$A = 1.58 \cdot 10^7 (1 + 100\Psi^2) \left(1 + \frac{1.33 \cdot 10^{-4}}{D^{1.5}}\right),$$

$$610 \quad \gamma = 0.5 - 0.25\Psi,$$

$$C = 7.08 \times 10^6 \psi$$

The above parameters adapted from Phillips et al. (2017a) concern planar crystals or snow with rimed fraction  $\Psi < 0.5$  that undergo fracturing:  $\Psi \leq 0.2$  corresponds to lightly rimed particles, while  $\Psi \approx 0.4$  represents highly rimed crystals/snow. The choice of the ice habit is based on particle images collected during the MAC flights, which indicate the presence of  
 615 needles and planar particles (O'Shea et al., 2017); needles are often considered secondary ice (Field et al., 2017). However, the M05 scheme does not explicitly consider habit and assumes spherical particles for all processes except sedimentation, for which the fallspeed-diameter relationships are for non-spherical ice.

For graupel-graupel collisions the parameters implemented in Eq. (16) are somewhat  
 620 different (Phillips et al., 2017a):

$$A = \frac{a_o}{3} + \max\left(\frac{2a_o}{3} - \frac{a_o}{9} |T - 258|, 0\right)$$

$$\gamma = 0.3,$$

$$C = 6.3 \times 10^6 \psi$$

Finally, an upper limit for the number of fragments produced per collision is imposed, set to  $F_{BRmax} = 100$ ; this is the same for all collision types (Phillips et al., 2017a).

625 We estimate the production rate of fragments for cloud ice-snow collisions and cloud ice-graupel collisions using Eq. (3) or (4) and one of the proposed formulations for  $F_{BR}$  above:  $\frac{dN_{iis}}{dt} F_{BR}$  and  $\frac{dN_{iig}}{dt} F_{BR}$ . For both of these collision types we assume that the cloud ice particles undergo break-up and the new smaller ice fragments remain within the same ice particle category. For snow-graupel collisions, where the snow particle is assumed to undergo

630 fracturing, the production term  $\frac{dN_{isg}}{dt} F_{BR}$  is added to the cloud ice category. In this case mass  
transfer from the snow to the cloud ice category also occurs, but according to Phillips et al.  
(2017a) this is only 0.1% of the snow mass that collides with graupel (5). Snow-snow and  
635 graupel-graupel collisions are handled in the same way:  $\frac{dN_{iss}}{dt} F_{BR}$  and  $\frac{dN_{igg}}{dt} F_{BR}$  are added to  
the cloud ice number equation, while 0.1% of  $\frac{dQ_{iss}}{dt}$  (11) and  $\frac{dQ_{igg}}{dt}$  (13) is added to the  
corresponding mass equation.

**Code and data availability:** MAC data are available at  
<https://catalogue.ceda.ac.uk/uuid/da17dab196f74d64af3ccbc35624027b>. The modified  
Morrison scheme is available upon request

640

**Competing interests:** The authors declare that they have no conflict of interest.

**Author contribution:** GS and AN conceived and led this study. EV helped with the model  
configuration and set-up, and provided Fig. 1. GY provided the observations and the model  
645 set-up for the MAC case. SJO post-processed MAC data. GS implemented the BR  
parameterizations, performed the WRF simulations, analyzed the results and, together with  
AN, led the manuscript writing. All authors contributed to the scientific interpretation,  
discussion and writing of the manuscript.

650 **Acknowledgements:** GS and AN acknowledge support from Laboratory of Atmospheric  
Processes and Their Impacts (LAPI) at the École Polytechnique Fédérale de Lausanne (EPFL)  
the project IC-IRIM (project ID 2018-01760) funded by the Swedish Research Council for  
Sustainable Development (FORMAS), the project PyroTRACH (ERC-2016-COG) funded  
655 from H2020-EU.1.1. - Excellent Science - European Research Council (project ID 726165)  
and the project FORCeS funded from Horizon H2020-EU.3.5.1. (project ID 821205). EV and  
AB acknowledge the financial support from EPFL-ENAC through the LOSUMEA project.  
The National Center for Atmospheric Research is sponsored by the U.S. National Science  
Foundation. GY acknowledges support from the UK Natural Environment Research Council  
(grant no.: NE/R009686/1). We are also grateful to MAC scientific crew for the observational  
660 datasets used in this study.

## References:

- 665 Baumgardner, D., Jonsson, H., Dawson, W., O'Connor, D., and R. Newton: The cloud, aerosol  
and precipitation spectrometer: A new instrument for cloud investigations. *Atmos. Res.*, 59,  
251–264. [https://doi.org/10.1016/S0169-8095\(01\)00119-3](https://doi.org/10.1016/S0169-8095(01)00119-3), 2001
- 670 Bodas-Salcedo, A., Williams, K. D., Ringer, M. A., Beau, I., Cole, J. N. S., Dufresne, J.-L., et  
al.: Origins of the solar radiation biases over the Southern Ocean in CFMIP2 Models, *J.*  
*Clim.*, 27, 41–56. <https://doi.org/10.1175/JCLI-D-13-00169.1>, 2014
- Bigg, E. K. : The formation of atmospheric ice crystals by the freezing of droplets. *Q. J. Roy.*  
*Meteorol. Soc.*, 79, 510–519. <https://doi.org/10.1002/qj.49707934207>, 1953
- 675 Bromwich, D. H., Otieno, F. O., Hines, K. M., Manning, K. W., and Shilo, E.: Comprehensive  
evaluation of polar weather research and forecasting model performance in the Antarctic,  
*Journal of Geophysical Research: Atmospheres*, 118, 274–292, doi:10.1029/2012jd018139,  
<http://dx.doi.org/10.1029/2012JD018139>, 2013.
- 680 Brown, P. and Francis, P.: Improved measurements of the ice water content in cirrus using a  
total-water probe, *J. Atmos. Ocean. Tech.*, 12, 410–414, 1995.
- Chen, F., and Dudhia, J.: Coupling an Advanced Land Surface–Hydrology Model with the  
Penn State– NCAR MM5 Modeling System. Part I: Model Implementation and Sensitivity.  
685 *Monthly Weather Rev.*, 129, 569–585, 2001.
- Choullarton, T. W., D. J. Griggs, B. Y. Humood, and Latham, J. : Laboratory studies of  
riming, and its relation to ice splinter production. *Quart. J. Roy. Meteor. Soc.*, 106, 367–374,  
doi:<https://doi.org/10.1002/qj.49710644809>, 1980.  
690
- Crosier, J., Choullarton, T. W., Westbrook, C. D., Blyth, A. M., Bower, K. N., Connolly, P. J.,  
Dearden, C., Gallagher, M. W., Cui, Z., and Nicol, J. C.: Microphysical properties of cold  
frontal rainbands, *Q. J. Roy. Meteorol. Soc.*, 140, 1257–1268, doi:10.1002/qj.2206, 2013.
- 695 Cooper, W.A.: Ice initiation in natural clouds. *Meteorological Monographs*, 21, 29–32.

<https://doi.org/10.1175/0065-9401-21.43.29>, 1986

700 Dee, D.P., Uppala, S.M., Simmons, A.J., Berrisford, P., Poli, P., Kobayashi, S., Andrae, U.,  
Balmaseda, M.A., Balsamo, G., Bauer, P., Bechtold, P., Beljaars, A.C.M., van de Berg, L.,  
Bidlot, J., Bormann, N., Delsol, C., Dragani, R., Fuentes, M., Geer, A.J., Haimberger, L.,  
705 Healy, S.B., Hersbach, H., Holm, E.V., Isaksen, I., Kalberg, P., Kohler, M., Matricardi, M.,  
McNally, A.P., Monge-Sanz, B.M., Morcrette, J.-J., Park, B.-K., Peubey, C., de Rosnay, P.,  
Tavolato, C., Thepaut, J.-N., Vitart, F.: The ERA-Interim reanalysis: Configuration and  
performance of the data assimilation system, *Q. J. Roy. Meteor. Soc.*, 137, 553–597,  
705 <https://doi.org/10.1002/qj.828>, 2011.

DeMott, P. J., Hill, T. C. J., McCluskey, C. S., Prather, K. A., Collins, D. B., Sullivan, R. C.,  
et al.: Sea spray aerosol as a unique source of ice nucleating particles. *Proceedings of the  
National Academy of Sciences*, 113(21), 5797–5803,  
710 <https://doi.org/10.1073/pnas.1514034112> (2016)

DeMott, P. J., Prenni, A. J., Liu, X., Kreidenweis, S. M., Petters, M. D., Twohy, C. H.,  
Richardson, M. S., Eidhammer, T., and Rogers, D. C.: Predicting global atmospheric ice  
nuclei distributions and their impacts on climate, *Proc. Nat. Acad. Sci.*,  
715 [doi:10.1073/pnas.0910818107](https://doi.org/10.1073/pnas.0910818107), 2010.

Field, P., Lawson, P., Brown, G., Lloyd, C., Westbrook, D., Moisseev, A., Miltenberger, A.,  
Nenes, A., Blyth, A., Choulaton, T., Connolly, P., Bühl, J., Crosier, J., Cui, Z., Dearden, C.,  
DeMott, P., Flossmann, A., Heymsfield, A., Huang, Y., Kalesse, H., Kanji, Z., Korolev, A.,  
720 Kirchgassner, A., Lasher-Trapp, S., Leisner, T., McFarquhar, G., Phillips, V., Stith, J., and  
Sullivan, S.: Chapter 7: Secondary ice production - current state of the science and  
recommendations for the future, *Meteor. Monogr.*, [doi:10.1175/AMSMONOGRAPHS-D-16-0014.1](https://doi.org/10.1175/AMSMONOGRAPHS-D-16-0014.1), 2017.

725 Flato, G., Marotzke, J., Abiodun, B., Braconnot, P., Chou, S., Collins, W., Cox, P., Driouech,  
F., Emori, S., Eyring, V., Forest, C., Gleckler, P., Guilyardi, E., Jakob, C., Kattsov, V.,  
Reason, C., and Rummukainen, M.: Evaluation of Climate Models. In: *Climate Change 2013:  
The Physical Science Basis. Contribution of Working Group I to the Fifth Assessment Report*

of the Intergovernmental Panel on Climate Change [Stocker, T.F., D. Qin, G.-K. Plattner, M. Tignor, S.K. Allen, J. Boschung, A. Nauels, Y. Xia, V. Bex and P.M. Midgley (eds.)], 2013.

730 Fridlind, A. M., Ackerman, A. S., McFarquhar, G., Zhang, G., Poellot, M. R., DeMott, P. J., Prenni, A. J., and Heymsfield, A. J.: Ice properties of single-layer stratocumulus during the Mixed-Phase Arctic Cloud Experiment: 2. Model results., *J. Geophys. Res.*, 112, D24202, <https://doi.org/10.1029/2007JD008646>, 2007.

735 Fu, S., Deng, X., Shupe, M.D., and Huiwen X.: A modelling study of the continuous ice formation in an autumnal Arctic mixed-phase cloud case, *Atmos. Res.*, 228, 77-85, <https://doi.org/10.1016/j.atmosres.2019.05.021>, 2019

740 Gilbert, E, Orr, A, King, JC, et al. Summertime cloud phase strongly influences surface melting on the Larsen C ice shelf, *Antarctica. Q J R Meteorol Soc.* 2020; 1-16. <https://doi.org/10.1002/qj.3753>

745 Glen, A., and Brooks, S. D.: A new method for measuring optical scattering properties of atmospherically relevant dusts using the Cloud and Aerosol Spectrometer with Polarization (CASPOL). *Atmospheric Chemistry & Physics*, 13, 1345–1356, <https://doi.org/10.5194/acp-13-1345-2013>, 2013

750 Grosvenor, D. P., Choularton, T. W., Lachlan-Cope, T., Gallagher, M. W., Crosier, J., Bower, K. N., Ladkin, R. S., and Dorsey, J. R.: In-situ aircraft observations of ice concentrations within clouds over the Antarctic Peninsula and Larsen Ice Shelf, *Atmos. Chem. Phys.*, 12, 11275–11294, <https://doi.org/10.5194/acp-12-11275-2012>, 2012.

755 Hallett, J. and Mossop, S. C.: Production of secondary ice particles during the riming process, *Nature*, 249, 26–28, doi:10.1038/249026a0, 1974.

760 Haynes, J.M., C. Jakob, W.B. Rossow, G. Tselioudis, and J. Brown: Major Characteristics of Southern Ocean Cloud Regimes and Their Effects on the Energy Budget. *J. Climate*, 24, 5061-5080, <https://doi.org/10.1175/2011JCLI4052.1>, 2011

Heymsfield, A.J., A. Bansemmer, and C.H. Twohy: Refinements to Ice Particle Mass

Dimensional and Terminal Velocity Relationships for Ice Clouds. Part I: Temperature Dependence. *J. Atmos. Sci.*, 64, 1047–1067, <https://doi.org/10.1175/JAS3890.1>, 2007

765

Hines, K. M., Bromwich, D. H., Wang, S.-H., Silber, I., Verlinde, J., and Lubin, D.: Microphysics of summer clouds in central West Antarctica simulated by the Polar Weather Research and Forecasting Model (WRF) and the Antarctic Mesoscale Prediction System (AMPS), *Atmos. Chem. Phys.*, 19, 12431–12454, <https://doi.org/10.5194/acp-19-12431-2019>, 2019.

770

Hoarau, T., Pinty, J.-P., and Barthe, C.: A representation of the collisional ice break-up process in the two-moment microphysics LIMA v1.0 scheme of Meso-NH, *Geosci. Model Dev.*, 11, 4269–4289, <https://doi.org/10.5194/gmd-11-4269-2018>, 2018.

775

Hyder, P., Edwards, J. M., Allan, R. P., Hewitt, H. T., Bracegirdle, T. J., Gregory, J. M., et al.: Critical Southern Ocean climate model biases traced to atmospheric model cloud errors. *Nature Communications*, 9, 3625. <https://doi.org/10.1038/s41467-018-05634-2>, 2018

Ikawa, M., and Saito, K.: Description of a Non-hydrostatic Model Developed at the Forecast Research Department of the MR, MRI Tech. Rep. 28, 238 pp, 1991

780

King J. C., Gadian, A., Kirchaessner, A., Kuipers, Munneke, P., Lachlan-Cope, T. A., Orr, A., Reijmer, C., van den Broeke, M. R., van Wessem, J. M., and Weeks, M.: Validation of the summertime surface energy budget of Larsen C Ice Shelf (Antarctica) as represented in three high-resolution atmospheric models, *J. Geophys. Res.*, 120, 1335–1347, <https://doi.org/10.1002/2014JD022604>, 2015.

785

King, J. C., Lachlan-Cope, T. A., Ladkin, R. S., and Weiss, A.: Airborne Measurements in the Stable Boundary Layer over the Larsen Ice Shelf, Antarctica, *Boundary-Layer Meteorology*, 127, 413–428, doi:10.1007/s10546-008-9271-4, 2008.

790

Klemp, J. B.: Advances in the WRF model for convection-resolving forecasting, *Adv. Geosci.*, 7, 25–29, <https://doi.org/10.5194/adgeo-7-25-2006>, 2006.

795

Korolev, A. V., Emery, E. F., Strapp, J.W., Cober, S. G., Isaac, G. A., Wasey, M., and Marcotte, D.: Small ice particles in tropospheric clouds: fact or artifact?, *B. Am. Meteorol.*



Soc., 92, 967–973, doi:10.1175/2010BAMS3141.1, 2011.

800 Korolev, A., Heckman, I., Wolde, M., Ackerman, A. S., Fridlind, A. M., Ladino, L., Lawson,  
P., Milbrandt, J., and Williams, E.: A new look at the environmental conditions favorable to  
secondary ice production, *Atmos. Chem. Phys. Discuss.*, <https://doi.org/10.5194/acp-2019-611>, in review, 2019.

805 Lachlan-Cope, T., Listowski, C., and O'Shea, S: The microphysics of clouds over the  
Antarctic peninsula—Part 1: Observations. *Atmos. Chem. Phys.*, 16(24), 15,605–15,617.  
<https://doi.org/10.5194/acp-16-15605-2016>, 2016

810 Lauber, A., Kiselev, A., Pander, T., Handmann, P., and Leisner, T.: Secondary ice formation  
during freezing of levitated droplets, *J. Atmos. Sci.*, 75, 2815–  
2826, <https://doi.org/10.1175/JAS-D-18-0052.1>, 2018.

815 Lawson, R. P., O'Connor, D., Zmarzly, P., Weaver, K., Baker, B., Mo, Q., and Jonsson, H. :  
The 2D-S (Stereo) probe: Design and preliminary tests of a new airborne, high-speed, high-  
resolution particle imaging probe. *Journal of Atmospheric and Oceanic Technology*, 23,  
1462–1477. <https://doi.org/10.1175/JTECH1927.1>, 2006

Lawson, P., Gurganus, C., Woods, S., and Brientjes, R.: Aircraft observations of cumulus  
microphysics ranging from the tropics to midlatitudes: implications for a “new” secondary ice  
process, *J. Atmos. Sci.*, 74, 2899–2920, <https://doi.org/10.1175/JAS-D-17-0033.1>, 2017.

820 Leisner, T., Pander, T., Handmann, P., and Kiselev, A.: Secondary ice processes upon  
heterogeneous freezing of cloud droplets, 14th Conf. on Cloud Physics and Atmospheric  
Radiation, Amer. Meteor. Soc, Boston, MA, 2014.

825 Listowski, C., and Lachlan-Cope, T.: The microphysics of clouds over the antarctic  
peninsula—Part 2:Modelling aspects within Polar WRF. *Atmos. Chem. Phys.*,17(17),  
10,195–10,221. <https://doi.org/10.5194/acp-17-10195-2017>, 2017

Listowski, C., Delanoë, J., Kirchgaessner, A., Lachlan-Cope, T., and King, J.: Antarctic  
clouds, supercooled liquid water and mixed phase, investigated with DARDAR: geographical

- 830 and seasonal variations, *Atmos. Chem. Phys.*, 19, 6771–6808, <https://doi.org/10.5194/acp-19-6771-2019>, 2019. Meyers, M. P., DeMott, P. J., and Cotton, W. R.: New primary ice-nucleation parameterizations in an explicit cloud model. *Journal of Applied Meteorology*, 31, 708–721. [https://doi.org/10.1175/1520-0450\(1992\)031<0708:NPINPI>2.0.CO;2](https://doi.org/10.1175/1520-0450(1992)031<0708:NPINPI>2.0.CO;2), 1992
- 835 McCluskey, C. S., Hill, T. C. J., Humphries, R. S., Rauker, A. M., Moreau, S., Stratton, P. G., Chambers, S. D., Williams, A. G., McRobert, I., Ward, J., Keywood, M.D., Harnwell, J., Ponsonby, W., Loh, Z.M., Krummel, P. B., Protat, A., Kreidenweis, S.M., and DeMott, P.J.: Observations of ice nucleating particles over Southern Ocean waters. *Geophysical Research Letters*, 45, 11,989–11,997. <https://doi.org/10.1029/2018GL079981>, 2018
- 840 Mizuno, H.: Parameterization of the accretion process between different precipitation elements. *J. Meteor. Soc. Japan*, 57, 273–281, 1990
- Mossop, S. C., and Hallett, J.: Ice crystal concentration in cumulus clouds: Influence of the drop spectrum. *Science*, 186, 632–634. <https://doi.org/10.1126/science.186.4164.632>, 1974.
- 845 Mossop, S. C. (1985). Secondary ice particle production during rime growth: The effect of drop size distribution and rimer velocity. *Quart. J. Roy. Meteor. Soc.*, 111(470), 1113–1124. <https://doi.org/10.1002/qj.49711147012>
- 850 Morrison, H., Curry, J.A., and Khvorostyanov, V.I.: A New Double-Moment Microphysics Parameterization for Application in Cloud and Climate Models. Part I: Description, *Atmos. Sci.*, 62, 3683–3704, 2005
- 855 Nakanishi, N., and Niino, H.: An improved Mellor–Yamada level-3 model: Its numerical stability and application to a regional prediction of advection fog. *Boundary-Layer Meteorology*, 119, 397–407, 2006
- 860 O’Shea, S. J., Choulaton, T. W., Flynn, M., Bower, K. N., Gallagher, M., Crosier, J., Williams, P., Crawford, I., Fleming, Z. L., Listowski, C., Kirchgaessner, A., Ladkin, R. S., and Lachlan-Cope, T.: In situ measurements of cloud microphysics and aerosol over coastal Antarctica during the MAC campaign, *Atmos. Chem. Phys.*, 17, 13049–13070, <https://doi.org/10.5194/acp-17-13049-2017>, 2017.

- 865 Passarelli, R.E.: An Approximate Analytical Model of the Vapor Deposition and Aggregation  
Growth of Snowflakes., *J. Atmos. Sci.*, 35, 118–124, 1978
- Phillips, V.T.J., Yano, J.-I., and Khain, A.: Ice multiplication by breakup in ice-ice collisions.  
Part I: Theoretical formulation, *J. Atmos. Sci.*, 74, 1705–1719, [https://doi.org/10.1175/JAS-D-](https://doi.org/10.1175/JAS-D-16-0224.1)  
870 16-0224.1, 2017a.
- Phillips, V.T.J., Yano, J.-I., Formenton, M., Ilotoviz, E., Kanawade, V., Kudzotsa, I., Sun, J.,  
Bansemer, A., Detwiler, A.G., Khain, A., and Tessoroff, S.A.: Ice Multiplication by  
Breakup in Ice–Ice Collisions. Part II: Numerical Simulations. *J. Atmos. Sci.*, 74, 2789–  
875 2811, <https://doi.org/10.1175/JAS-D-16-0223.1>, 2017b.
- Prein, A. F., Langhans, W., Fosser, G., Ferrone, A., Ban, N., Goergen, K., Keller, M., Tille,  
M., Gutjahr, O., Feser, F., Brisson, E., Kollet, S., Schmidli, J., Lipzig, N. P. M., and Leung,  
880 R.: A review on regional convection-permitting climate modeling: Demonstrations, prospects,  
and challenges, *Reviews of Geophysics*, 53(2), 323–361, doi:10.1002/2014RG000475, 2015.
- Pruppacher, H.R., and Klett, J.D. : *Microphysics of Clouds and Precipitation*. 2nd Edition,  
Kluwer Academic, Dordrecht, 954 p., 1997
- 885 Qu, Y., Khain, A., Phillips, V., Ilotoviz, E., Shpund, J., Patade, S., and Chen, B. : The role  
of ice splintering on microphysics of deep convective clouds forming under different aerosol  
conditions: Simulations using the model with spectral bin microphysics. *J. Geophys. Res.*  
*Atmos.*, 125, e2019JD031312. <https://doi.org/10.1029/2019JD031312>, 2020
- 890 Rangno, A.L., and Hobbs, P.V., Ice particles in stratiform clouds in the Arctic and possible  
mechanisms for the production of high ice concentrations, *J. Geophys. Res.*, 106, 15, 065–  
15,075, 2001.
- Reisner, J., Rasmussen, R. M., and Bruintjes, R. T.: Explicit forecasting of supercooled liquid  
895 water in winter storms using the MM5 mesoscale model, *Quart. J. Roy. Meteor. Soc.*,  
124(548), 1071–1107, doi: 10.1002/qj.49712454804, 1998.

- Skamarock, W. C., and Klemp, J. B.: A time-split nonhydrostatic atmospheric model for weather research and forecasting applications. *J. Comp. Phys.*, 227(7), 3465–3485.  
900 <https://doi.org/10.1016/j.jcp.2007.01.037>, 2008
- Schmale, J., Baccarini, A., Thurnherr, I., Henning, S., Efraim, A., Regayre, L., Bolas, C.,  
Hartmann, M., Welti, A., Lehtipalo, K., Aemisegger, F., Tatzelt, C., Landwehr, S., Modini, R.,  
905 L., Tummon, F., Johnson, J., Harris, N., Schnaiter, M., Toffoli, A., Derkani, M., Bukowiecki,  
35 N., Stratmann, F., Dommen, J., Baltensperger, U., Wernli, H., Rosenfeld, D., Gysel-Beer,  
M., and Carslaw, K.: Overview of the Antarctic Circumnavigation Expedition: Study of  
Preindustrial-like Aerosols and Their Climate Effects (ACE-SPACE), *Bull. Amer. Meteor.  
Soc.*, 100 (11): 2260–2283, DOI:10.1175/BAMS-18-0187.1, 2019
- 910 Schwarzenboeck, A., Shcherbakov, V., Lefevre, R., Gayet, J.-F., Duroure, C., and Pointin, Y.:  
Indications for stellar-crystal fragmentation in Arctic clouds, *Atmos. Res.*, 92, 220  
228, <https://doi.org/10.1016/j.atmosres.2008.10.002>, 2009.
- Sotiropoulou, G., Sullivan, S., Savre, J., Lloyd, G., Lachlan-Cope, T., Ekman, A. M. L., and  
Nenes, A.: The impact of Secondary Ice Production on Arctic Stratocumulus, *Atmos. Chem.*  
915 *Phys.*, 20, 1301–1316, <https://doi.org/10.5194/acp-2019-804>, 2020.
- Stephens, G.L.: Radiation profiles in extended water clouds. II. Parameterization schemes. *J.*  
*Atmos. Sci.*, 35, 2123–2132, 1978
- 920 Sullivan, S. C., Kiselev, A., Leisner, T., Hoose, C., and Nenes, A.: Initiation of secondary ice  
production in clouds, *Atmos. Chem. Phys.*, 18, 1593–1610, doi:10.5194/acp-18-1593-2018,  
2018a.
- Sullivan, S. C., Barthlott, C., Crosier, J., Zhukov, I., Nenes, A., and Hoose, C.: The effect of  
925 secondary ice production parameterization on the simulation of a cold frontal rainband,  
*Atmos. Chem. Phys.*, 18, 16461–16480, <https://doi.org/10.5194/acp-18-16461-2018>, 2018b.
- Takahashi, T., Nagao, Y., and Kushiyama, Y.: Possible high ice particle production during  
graupel-graupel collisions, *J. Atmos. Sci.*, 52, 4523–4527, doi:10.1175/1520-0469, 1995.

930 Vardiman, L.: The generation of secondary ice particles in clouds by crystal-crystal collision, *J. Atmos. Sci.*, 35, 2168–2180, doi:10.1175/1520-0469, 1978.

Verlinde, J., Flatau, P.J, and W.R. Cotton, W.R.: Analytical Solutions to the Collection Growth Equation: Comparison with Approximate Methods and Application to Cloud  
935 Microphysics Parameterization Schemes. *J. Atmos. Sci.*, 47, 2871–2880, [https://doi.org/10.1175/1520-0469\(1990\)047<2871:ASTTCG>2.0.CO;2](https://doi.org/10.1175/1520-0469(1990)047<2871:ASTTCG>2.0.CO;2)

Verlinde, J. and W.R. Cotton, 1993: Fitting Microphysical Observations of Nonsteady  
940 Convective Clouds to a Numerical Model: An Application of the Adjoint Technique of Data Assimilation to a Kinematic Model. *Mon. Wea. Rev.*, 121, 2776–2793, [https://doi.org/10.1175/1520-0493\(1993\)121<2776:FMOONC>2.0.CO;2](https://doi.org/10.1175/1520-0493(1993)121<2776:FMOONC>2.0.CO;2)

Vignon, É., Besic, N., Jullien, N., Gehring, J., & Berne, A. Microphysics of snowfall over coastal East Antarctica simulated by Polar WRF and observed by radar. *J. Geophys. Res.: Atmospheres*, 124, 11452–11476, 2019.

945 Welti, A., Bigg, E. K., DeMott, P. J., Gong, X., Hartmann, M., Harvey, M., Henning, S., Herenz, P., Hill, T. C. J., Hornblow, B., Leck, C., Löffler, M., McCluskey, C. S., Rauker, A. M., Schmale, J., Tatzelt, C., van Pinxteren, M., and Stratmann, F.: Shipbased measurements of ice nuclei concentrations over the Arctic, Atlantic, Pacific and Southern Ocean, *Atmos. Chem. Phys. Discuss.*, <https://doi.org/10.5194/acp-2020-466>, in review, 2020.  
950

Yano, J.-I. and Phillips, V. T. J.: Ice-ice collisions: an ice multiplication process in atmospheric clouds, *J. Atmos. Sci.*, 68, 322–333, doi:10.1175/2010JAS3607.1, 2011.

955 Yano, J.-I., Phillips, V. T. J., and Kanawade, V.: Explosive ice multiplication by mechanical break-up in-ice-ice collisions: a dynamical system-based study, *Q. J. Roy. Meteor. Soc.*, 142, 867–879, <https://doi.org/10.1002/qj.2687>, 2016.

Young, G., Lachlan-Cope, T., O'Shea, S. J., Dearden, C., Listowski, C., Bower, K. N.,  
960 Choularton T.W., and Gallagher M.W.: Radiative effects of secondary ice enhancement in coastal Antarctic clouds. *Geophys. Res. Lett.*, 46, 23122321, <https://doi.org/10.1029/2018GL080551>, 2019.

Young, K. C., 1974: The Role of Contact Nucleation in Ice Phase Initiation in Clouds. *J. Atmos. Sci.*, 31, 768–776, [https://doi.org/10.1175/1520-0469\(1974\)031<0768:TROCNI>2.0.CO;2](https://doi.org/10.1175/1520-0469(1974)031<0768:TROCNI>2.0.CO;2).

965

**Tables:**

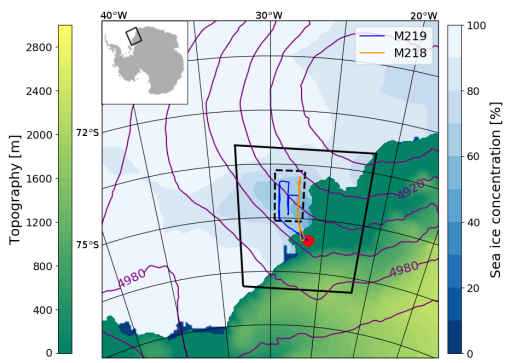
970

**Table 1:** Mean modeled downward and upward shortwave ( $SWD_{SFC}$ ,  $SWU_{SFC}$ ) and longwave ( $LWD_{SFC}$ ,  $LWU_{SFC}$ ) surface radiation, along with upward shortwave and longwave ( $SWU_{TOA}$ ,  $LWU_{TOA}$ ) radiation at the top of the atmosphere, during flights M218 and M219. Model results are averaged over the dashed rectangular area in Fig. 1.

975

Simulation	$SWD_{SFC}$ ( $Wm^{-2}$ )	$SWU_{SFC}$ ( $Wm^{-2}$ )	$LWD_{SFC}$ ( $Wm^{-2}$ )	$LWU_{SFC}$ ( $Wm^{-2}$ )	$SWU_{TOA}$ ( $Wm^{-2}$ )	$LWU_{TOA}$ ( $Wm^{-2}$ )
CNTRL	323.9	182.1	244.3	304.6	255.8	218.4
PHIL0.2	328.6	184.5	244.1	304.6	254.8	218.5
PHIL0.3	322.3	181.0	247.4	305.3	256.6	217.9
PHIL0.4	339.7	190.8	243.3	304.9	251.1	219.8
FRAG1	354.1	198.6	236.7	303.8	246.9	221.5
FRAG1siz	335.7	188.8	244.0	304.6	250.5	220.7
TAKAH	365.9	206.5	229.8	303.3	242.5	221.2
TAKAHsc	349.5	194.5	237.0	304.2	246.6	222.0

**Figures:**



980

**Figure 1:** Map of Antarctic domains. Colors indicate terrain heights (green to yellow) and sea-ice concentrations (blue to white), whereas the purple contours correspond to 500 hPa geopotential heights from the CNTRL simulation at 18:00 UTC, 27 November 2015. The black solid line delimits the 1-km horizontal grid spacing domain, while the dashed one outlines the subset of the nest used for direct comparison with the aircraft data. Orange and blue lines indicate the flight tracks, while the red circle represents Halley station. The small figure in the top right corner indicates the location of the 1-km horizontal grid spacing domain relative to the Antarctic continent.

990

995

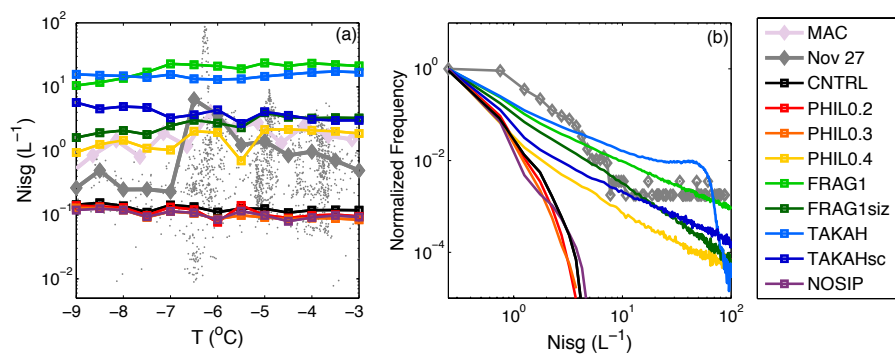


**Figure 2:** (a) Mean ice number concentrations (cloud ice + snow + graupel,  $N_{ice}$ ) as a function of temperature for the whole MAC campaign (pink), our case study (grey) and the eight model simulations. Grey dots indicate point observations. (b) Relative frequency distribution of  $N_{ice}$ , binned in  $0.5 L^{-1}$  intervals, scaled with maximum frequency. Ice properties are calculated for particles  $> 80 \mu m$  and for  $N_{ice} > 0.005 L^{-1}$  within the lowest 1.5 km a.s.l.

1005

1010



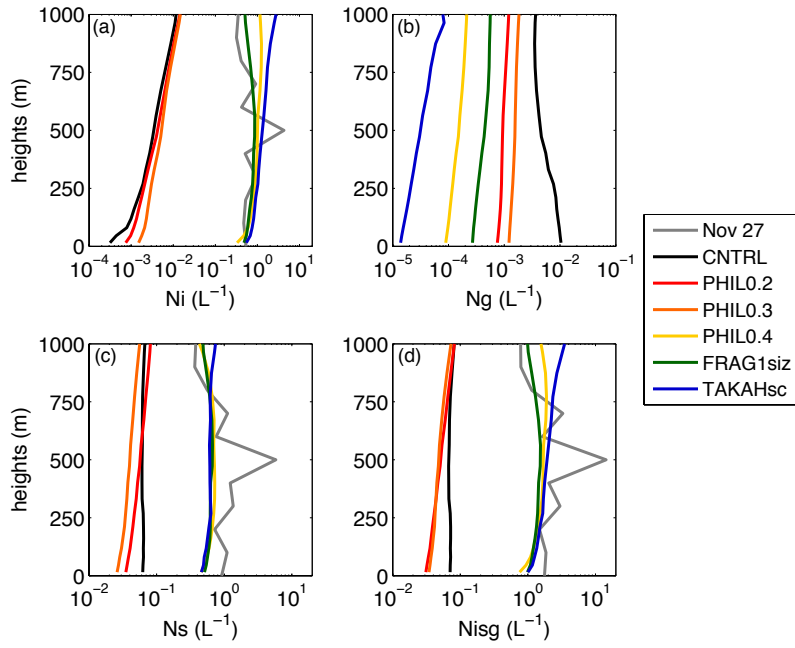


**Figure 3:** Mean vertical profiles of number concentrations of modeled (a) cloud ice, (b) graupel, (c) snow and (d) total ICNCS for six simulations. Grey lines represent measured concentrations with diameters (a) smaller and (c) larger than 250  $\mu\text{m}$ . Graupel concentrations cannot be distinguished in the measurements (hence no grey profile in panel b). Ice properties from the model are calculated for  $N_{\text{isg}} > 0.005 \text{ L}^{-1}$ . For consistency with observations, only particles with sizes  $> 80 \mu\text{m}$  are included in the modeled profiles in panels (a), (c) and (d).

1020

1025

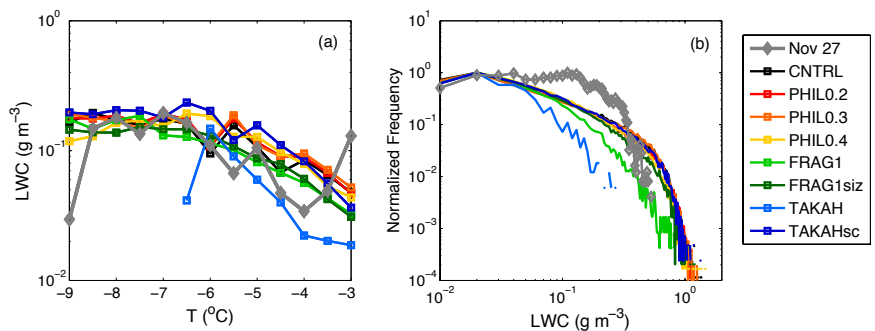


**Figure 4:** (a) Mean liquid water content (LWC) as a function of temperature for our case study (grey) and the eight model simulations. (b) Relative frequency distribution of LWC, binned in  $0.01 \text{ g m}^{-3}$  intervals, scaled with maximum frequency. Only values greater than  $0.01 \text{ g m}^{-3}$  within the lowest 1.5 km a.s.l. are included in the analysis.

1035

1040

1045

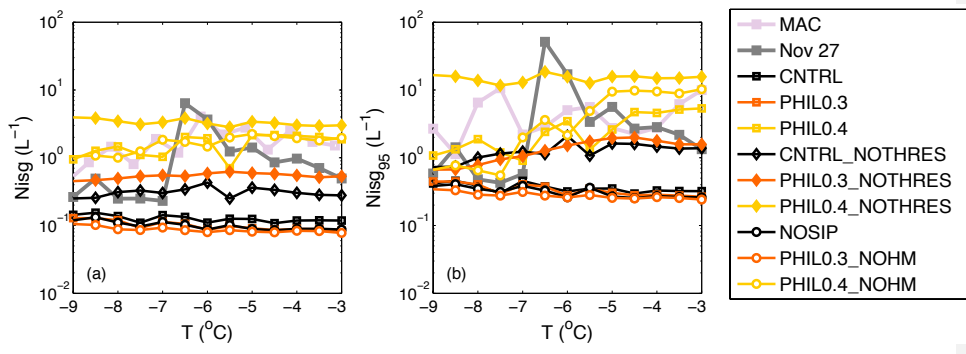
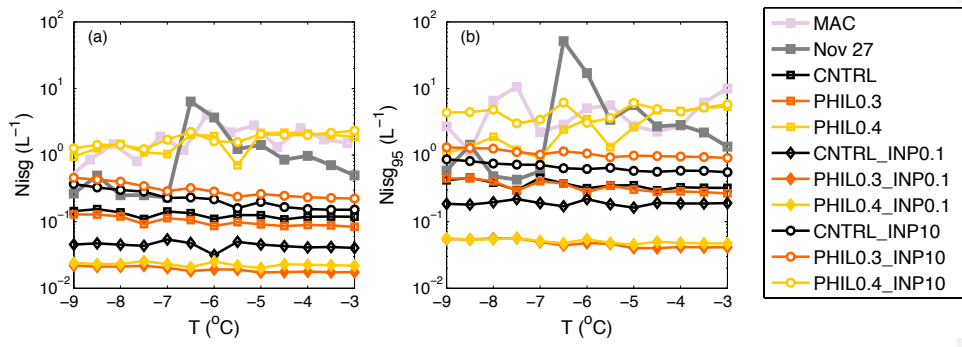


**Figure 5:** Total ice number concentrations ( $N_{isg}$ ) for particles  $> 80 \mu\text{m}$  as a function of temperature for the while MAC campaign (pink), our case study (grey) and the nine sensitivity simulations with varying treatment of the H-M process (see section 4.3). Mean values and the 95<sup>th</sup> percentile are shown in panels (a) and (b), respectively.

1055

1060

1065



1070 **Figure 6:** Same as in Fig. 5 but for sensitivity simulations with varying INP conditions (see  
 1075 section 4.4)

1075

1080